Closed-form expressions for effective constitutive parameters: Electrostrictive and magnetostrictive tensors for bianisotropic metamaterials and their use in optical force density calculations

Neng Wang,[1] Shubo Wang,[1,2] Zhao-Qing Zhang,[1] and C. T. Chan[1,*]
[1]*Department of Physics, The Hong Kong University of Science and Technology, Hong Kong, China*
[2]*Department of Physics, City University of Hong Kong, Hong Kong, China*

(Received 28 November 2017; revised manuscript received 14 May 2018; published 25 July 2018)

Using a multiple scattering technique, we derived closed-form expressions for effective constitutive parameters and electro/magneto-strictive tensor components for 2D bianisotropic metamaterials. Using the principle of virtual work, we obtained the electromagnetic stress tensor that can be used to calculate the optical force density inside such media. The analytic expressions are tested against full wave numerical simulations. Our effective medium theory is essential for providing a complete macroscopic description of the optical and opto-mechanical properties of bianisotropic composites.

DOI: 10.1103/PhysRevB.98.045426

I. INTRODUCTION

Metamaterials are artificial composite materials carrying subwavelength inclusions. These materials are designed to have optical or acoustic properties that are not found in nature and hence can be employed to realize novel phenomena that were once thought to be impossible, such as negative refraction [1–3] and cloaking [4–8]. The unusual properties of metamaterials are frequently attributed to their unconventional constitutive parameters, which can be very different from those of the constitutive components. As the properties of metamaterials are characterized by macroscopic constitutive parameters, it is essential to find good effective medium theories that can produce accurate descriptions of the composite material so that we do not need to worry about the complex structural details at the subwavelength level.

Developing analytic effective medium approximations is often challenging, particularly for anisotropic composites whose scattering properties are complicated and effective constitutive parameters are tensors rather than scalars [9–15]. Bianisotropic metamaterials, which have attracted a lot of attention due to their intriguing wave manipulating properties recently, such as negative refraction [16–18], strong optical chirality [19–24], and serving as a platform for realizing nontrivial topological phenomena [25,26], frequently have complex underlying structures. Building an effective medium theory (EMT) for them is not easy, since their scattering properties are determined by the complex interplay between different components of effective constitutive tensors. In the past decades, considerable efforts have been made to calculate the effective constitutive parameters for the bianisotropic metamaterials which are based on parameter retrieval [27–31]. In this paper, we will use analytic techniques to formulate an effective medium approach for 2D bianisotropic metamaterials. Our approach is complete in the sense that it not only provides the usual constitutive parameters that can calculate scattering and absorption, but also provides enough information to evaluate microscopic details such as the optical force density inside the metamaterial, which is known to be more difficult to calculate than the total force. Such capability enables us to consider the optomechanical response of such materials, in particular soft composites which can be deformed in light fields due to the nonuniform optical force distribution [32–34].

Using multiple scattering theory (MST), we analytically derived the macroscopic effective parameters as well as the electro/magneto-strictive tensors for these materials. The electrostrictive and magnetostrictive tensors describe the response of effective constitutive parameters under deformation, which depend on not only the filling ratio but also the lattice symmetry. We note that most methods used in EMT, such as coherent potential approximation [35,36] and the layer Korringa-Kohn-Rostoker method [37–39], cannot derive the electrostrictive and magnetostrictive tensors correctly because the symmetry of microstructure is not considered. However, MST incorporates the symmetry of the microstructure, and hence the electrostrictive and magnetostrictive tensors can be correctly obtained. Using the virtual work method, we derived the electromagnetic (EM) stress tensor (called extended Helmholtz stress tensor thereafter) for bianisotropic media, which can be used to calculate the optical force density inside a bianisotropic metamaterial with complex structures. We note that traditional effective medium theories do not provide sufficient information to study the optical force density because they do not give expressions for the electro/magneto-strictive tensor components. By comparing the results produced by different stress tensors, we demonstrate that the extended Helmholtz stress tensor gives the most accurate description of optical force density in bianisotropic metamaterials.

II. THE EFFECTIVE CONSTITUTIVE PARAMETERS

The bianisotropic metamaterials considered in this study consist of identical chiral inclusions (can having complex underlying structures) arranged into a regular or random lattice in the xy plane embedded in air with permittivity ε_0 and

*Corresponding author: phchan@ust.hk

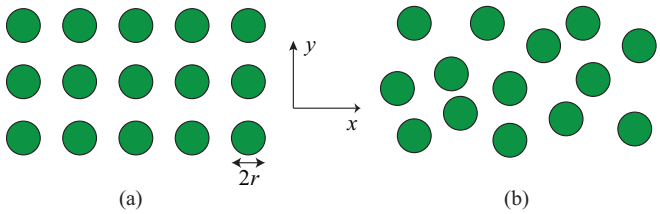

FIG. 1. Top view of the bianisotropic metamaterial with parallel cylindrical inclusions arranged in either (a) regular or (b) random lattice in the xy plane. The Mie coefficients of cylindrical inclusions satisfy $A_n = A_{-n}$, $B_n = B_{-n}$, and $C_n = C_{-n}$ and the background is isotropic and achiral.

permeability μ_0, as shown schematically in Fig. 1. In the long-wavelength limit, the effective relative constitutive parameters of the metamaterials have diagonal matrix forms as

$$\overleftrightarrow{\varepsilon}_e = \varepsilon_t\hat{x}\hat{x} + \varepsilon_t\hat{y}\hat{y} + \varepsilon_z\hat{z}\hat{z}, \quad \overleftrightarrow{\mu}_e = \mu_t\hat{x}\hat{x} + \mu_t\hat{y}\hat{y} + \mu_z\hat{z}\hat{z},$$
$$\overleftrightarrow{\kappa}_e = \kappa_t\hat{x}\hat{x} + \kappa_t\hat{y}\hat{y} + \kappa_z\hat{z}\hat{z}, \tag{1}$$

where $\overleftrightarrow{\varepsilon}_e$, $\overleftrightarrow{\mu}_e$, and $\overleftrightarrow{\kappa}_e$ are the effective relative permittivity, permeability and chirality tensors, respectively. According to Maxwell equations, we have the wave equation for the out-of-plane EM fields inside such a metamaterial as

$$k^2\begin{pmatrix} E_z \\ H_z \end{pmatrix} = \omega^2\begin{pmatrix} \varepsilon_z\mu_t + \kappa_z\kappa_t & i\mu_t\kappa_z + i\mu_z\kappa_t \\ -i\varepsilon_t\kappa_z - i\varepsilon_z\kappa_t & \varepsilon_t\mu_z + \kappa_z\kappa_t \end{pmatrix}\begin{pmatrix} E_z \\ H_z \end{pmatrix}, \tag{2}$$

which directly leads to the two eigenmodes with corresponding wave numbers expressed as

$$K_\pm^2 = k_0^2\frac{\varepsilon_z\mu_t + \varepsilon_t\mu_z + 2\kappa_z\kappa_t \pm \sqrt{(\varepsilon_z\mu_t - \varepsilon_t\mu_z)^2 + 4\kappa_z\kappa_t(\varepsilon_z\mu_t + \varepsilon_t\mu_z) + 4\kappa_z^2\varepsilon_t\mu_t + 4\kappa_t^2\varepsilon_z\mu_z}}{2}. \tag{3}$$

From Eq. (3), we easily obtain the following relationships:

$$K_+^2K_-^2 = k_0^4\left(\varepsilon_z\mu_z - \kappa_z^2\right)\left(\varepsilon_t\mu_t - \kappa_t^2\right), \tag{4}$$

where the wave number product can be factorized into two parts involving the out-of-plane (with subscript z) and in-plane (with subscript t) constitutive parameters, respectively, and k_0 is the wave number in air.

The dispersion relation for a periodic system can be obtained by considering the secular equation derived from the MST. In the following, we will analytically derive the expressions of the Mie coefficients of the isotropic chiral cylinders and the secular equation using the MST.

A. Mie coefficients for isotropic chiral cylinders

Consider the scattering of electromagnetic wave by a single chiral cylinder. The cylinder is isotropic with the constitutive relations given by

$$\mathbf{D} = \varepsilon\varepsilon_0\mathbf{E} + i\kappa/c\mathbf{H}, \mathbf{B} = \mu\mu_0\mathbf{H} - i\kappa/c\mathbf{E},$$

where ε, μ, and κ are the relative permittivity, permeability and chirality of the cylinder. Using the Mie scattering method [40], the incident fields ($\mathbf{E}_i$, $\mathbf{H}_i$), scattered field ($\mathbf{E}_s$, $\mathbf{H}_s$) and the field inside the chiral cylinder ($\mathbf{E}_{\rm ins}$, $\mathbf{H}_{\rm ins}$) at a location $\mathbf{r} = (r, \phi)$(the origin is located at the center of the cylinder) can be written as

$$\mathbf{E}_i = \sum_{n=-\infty}^{\infty}\left[q_n\mathbf{N}_n^{(1)}(k_0, \mathbf{r}) + p_n\mathbf{M}_n^{(1)}(k_0, \mathbf{r})\right],$$
$$\mathbf{H}_i = -i\sqrt{\frac{\varepsilon_0}{\mu_0}}\sum_{n=-\infty}^{\infty}\left[p_n\mathbf{N}_n^{(1)}(k_0, \mathbf{r}) + q_n\mathbf{M}_n^{(1)}(k_0, \mathbf{r})\right],$$
$$\mathbf{E}_s = -\sum_{n=-\infty}^{\infty}\left[b_n\mathbf{N}_n^{(3)}(k_0, \mathbf{r}) + a_n\mathbf{M}_n^{(3)}(k_0, \mathbf{r})\right],$$
$$\mathbf{H}_s = i\sqrt{\frac{\varepsilon_0}{\mu_0}}\sum_{n=-\infty}^{\infty}\left[a_n\mathbf{N}_n^{(3)}(k_0, \mathbf{r}) + b_n\mathbf{M}_n^{(3)}(k_0, \mathbf{r})\right],$$

$$\mathbf{E}_{\rm ins} = \sum_{n=-\infty}^{\infty}\left[c_n\mathbf{N}_n^{(1)}(k_1, \mathbf{r}) + c_n\mathbf{M}_n^{(1)}(k_1, \mathbf{r}) + d_n\mathbf{N}_n^{(1)}(k_2, \mathbf{r}) - d_n\mathbf{M}_n^{(1)}(k_2, \mathbf{r})\right],$$
$$\mathbf{H}_{\rm ins} = -i\sqrt{\frac{\varepsilon_0\varepsilon}{\mu_0\mu}}\sum_{n=-\infty}^{\infty}\left[c_n\mathbf{N}_n^{(1)}(k_1, \mathbf{r}) + c_n\mathbf{M}_n^{(1)}(k_1, \mathbf{r}) - d_n\mathbf{N}_n^{(1)}(k_2, \mathbf{r}) + d_n\mathbf{M}_n^{(1)}(k_2, \mathbf{r})\right], \tag{5}$$

where $k_{1,2} = (\sqrt{\varepsilon\mu} \pm \kappa)k_0$ are wavenumbers inside the chiral cylinder, p_n, q_n, a_n, b_n and c_n, d_n are the expansion coefficients for the incident field, scattered field and field inside the cylinder, respectively, and $\mathbf{M}_n^{(J)}$, $\mathbf{N}_n^{(J)}$ are the vector cylindrical wave functions [40], which are expressed as

$$\mathbf{M}_n^{(J)}(k, \mathbf{r}) = \left[\frac{in}{kr}z_n^{(J)}(kr)\mathbf{e}_r - z_n^{(J)\prime}(kr)\mathbf{e}_\phi\right]e^{in\phi},$$
$$\mathbf{N}_n^{(J)}(k, \mathbf{r}) = z_n^{(J)}(kr)e^{in\phi}\mathbf{e}_z$$

with $z_n^{(1)}(kr) = J_n(kr)$, $z_n^{(1)\prime}(kr) = J_n'(kr)$ denoting the Bessel function and its derivative with respect to its argument, and $z_n^{(3)}(kr) = H_n^{(1)}(kr)$, $z_n^{(3)\prime}(kr) = H_n^{(1)\prime}(kr)$ denoting the Hankel function of first kind and its derivative with respect to its argument. The expansion coefficients are related by [40]

$$a_n = A_np_n + C_nq_n, \quad b_n = C_np_n + B_nq_n, \tag{6}$$

where A_n, B_n, and C_n are the Mie coefficients corresponding to electric, magnetic and chirality parts, respectively. Employing the boundary conditions that the tangential components of the electromagnetic fields should be continuous, we have

$$q_nJ_n(x_0) - b_nH_n^{(1)}(x_0) = c_nJ_n(x_1) + d_nJ_n(x_2),$$
$$p_nJ_n'(x_0) - a_nH_n^{(1)\prime}(x_0) = c_nJ_n'(x_1) - d_nJ_n'(x_2),$$
$$p_nJ_n(x_0) - a_nH_n^{(1)}(x_0) = \sqrt{\frac{\varepsilon}{\mu}}[c_nJ_n(x_1) - d_nJ_n(x_2)],$$
$$q_nJ_n'(x_0) - b_nH_n^{(1)\prime}(x_0) = \sqrt{\frac{\varepsilon}{\mu}}[c_nJ_n'(x_1) + d_nJ_n'(x_2)], \tag{7}$$

where $x_{0,1,2} = k_{0,1,2} r_0$ are dimensionless size parameters with r_0 being the radius of the cylinder. Then the Mie coefficients for all orders can be obtained by solving Eq. (7). In the long-wavelength limit that $x_0 \ll 1$, remaining only the lowest order of x_0, the zeroth and first-order Mie coefficients are reduced to

$$\begin{aligned} A_0 &= \frac{i}{4}(1-\mu)\pi x_0^2, \quad A_{\pm 1} = -\frac{i}{4}\frac{1+\varepsilon-\mu+\varepsilon\mu-\kappa^2}{1+\varepsilon+\mu+\varepsilon\mu-\kappa^2}\pi x_0^2, \\ B_0 &= \frac{i}{4}(1-\varepsilon)\pi x_0^2, \quad B_{\pm 1} = -\frac{i}{4}\frac{1-\varepsilon+\mu+\varepsilon\mu-\kappa^2}{1+\varepsilon+\mu+\varepsilon\mu-\kappa^2}\pi x_0^2, \\ C_0 &= -\frac{i}{4}\kappa\pi x_0^2, \quad C_{\pm 1} = -\frac{i}{2}\frac{\kappa}{1+\varepsilon+\mu+\varepsilon\mu-\kappa^2}\pi x_0^2. \end{aligned} \tag{8}$$

B. Multiple scattering formulism for bianisotropic cylinders

In this subsection, we will derive the secular equation for a lattice of chiral cylinders starting from the MST. Here we consider a much more general case that the chiral cylinders do not need to be isotropic. According to the Mie theory, the scattering properties can still be described by the Mie coefficients A_n, B_n, C_n which now can become very complicated and cannot be simply expressed in a closed form as in Eq. (8). The only condition must be fulfilled is $A_n = A_{-n}$, $B_n = B_{-n}$, and $C_n = C_{-n}$ for $n = 0, 1$, which is true when the constitutive parameters of the cylinders are given by Eq. (1).

For a 2D periodic system with multiple scattering between the cylinders, the incident field acting on an arbitrary cylinder j also includes the scattering fields from other cylinders, which can be written as

$$\begin{aligned} \mathbf{E}_i(j) &= -\sum_{l\neq j}\sum_{m=-\infty}^{\infty}\left[a_m^l \mathbf{M}_m^{(3)}(k_0, \mathbf{r}-\mathbf{r}_l) + b_m^l \mathbf{N}_m^{(3)}(k_0, \mathbf{r}-\mathbf{r}_l)\right], \\ \mathbf{H}_i(j) &= i\sqrt{\frac{\varepsilon_0}{\mu_0}}\sum_{l\neq j}\sum_{m=-\infty}^{\infty}\left[b_m^l \mathbf{M}_m^{(3)}(k_0, \mathbf{r}-\mathbf{r}_l) + a_m^l \mathbf{N}_m^{(3)}(k_0, \mathbf{r}-\mathbf{r}_l)\right], \end{aligned} \tag{9}$$

where a_m^l, b_m^l, and $\mathbf{r}_l$ are scattering coefficients and location of cylinder l. Using the translation additional theorem [41]

$$\begin{aligned} \mathbf{M}_m^{(3)}(k_0, \mathbf{r}-\mathbf{r}_l) &= \sum_n H_{m-n}^{(1)}(kd_{lj}) e^{-i(n-m)\phi_{lj}} \mathbf{M}_n^{(1)}(k_0, \mathbf{r}-\mathbf{r}_j), \\ \mathbf{N}_m^{(3)}(k_0, \mathbf{r}-\mathbf{r}_l) &= \sum_n H_{m-n}^{(1)}(kd_{lj}) e^{-i(n-m)\phi_{lj}} \mathbf{N}_n^{(1)}(k_0, \mathbf{r}-\mathbf{r}_j), \end{aligned} \tag{10}$$

where $\mathbf{r}_{lj}{=}\mathbf{r}_j - \mathbf{r}_l = (d_{lj}, \phi_{lj})$ is the vector that directs from cylinder j to cylinder l and imposing the Bloch condition in the periodic structure:

$$a_m^l = a_m^j e^{i\mathbf{K}\cdot\mathbf{r}_{lj}}, \quad b_m^l = b_m^j e^{i\mathbf{K}\cdot\mathbf{r}_{lj}},$$

where $\mathbf{K} = (K, \phi_K)$ is the Bloch vector, the incident fields can be rewritten as

$$\begin{aligned} \mathbf{E}_i(j) &= -\sum_{n=-\infty}^{\infty}\left[\sum_{m=-\infty}^{\infty} a_m^j S_{m-n} \mathbf{M}_n^{(1)}(k_0, \mathbf{r}-\mathbf{r}_j) + \sum_{m=-\infty}^{\infty} b_m^j S_{m-n} \mathbf{N}_n^{(1)}(k_0, \mathbf{r}-\mathbf{r}_j)\right], \\ \mathbf{H}_i(j) &= i\sqrt{\frac{\varepsilon_0}{\mu_0}}\sum_{n=-\infty}^{\infty}\left[\sum_{m=-\infty}^{\infty} b_m^j S_{m-n} \mathbf{M}_n^{(1)}(k_0, \mathbf{r}-\mathbf{r}_j) + \sum_{m=-\infty}^{\infty} a_m^j S_{m-n} \mathbf{N}_n^{(1)}(k_0, \mathbf{r}-\mathbf{r}_j)\right], \end{aligned} \tag{11}$$

where S_{m-n} is the lattice sum defined as

$$S_{m-n} = \sum_{l\neq j} e^{i\mathbf{K}\cdot\mathbf{r}_{lj}} H_{m-n}^{(1)}(kd_{lj}) e^{-i(n-m)\phi_{lj}}, \quad S_{n-m} = -(S_{m-n})^*.$$

Then we have the self-consistent equations

$$a_n^j = \sum_{m=-\infty}^{\infty}\left(A_n a_m^j S_{m-n} + C_n b_m^j S_{m-n}\right), \quad b_n^j = \sum_{m=-\infty}^{\infty}\left(C_n a_m^j S_{m-n} + B_n b_m^j S_{m-n}\right). \tag{12}$$

The dispersion relation $\omega(\mathbf{K})$ is obtained from the condition that gives nontrivial solutions to Eq. (12) [42]. Up to dipole orders, the secular equation is reduced to

$$\det\begin{vmatrix} A_1S_0+1 & A_1S_{-1} & A_1S_{-2} & C_1S_0 & C_1S_1 & C_1S_{-2} \\ A_0S_1 & A_0S_0+1 & A_0S_{-1} & C_0S_1 & C_0S_0 & C_0S_{-1} \\ A_1S_2 & A_1S_1 & A_1S_0+1 & C_1S_2 & C_1S_1 & C_1S_0 \\ C_1S_0 & C_1S_{-1} & C_1S_{-2} & B_1S_0+1 & B_1S_{-1} & B_1S_{-2} \\ C_0S_1 & C_0S_0 & C_0S_{-1} & B_0S_1 & B_0S_0+1 & B_0S_{-1} \\ C_1S_2 & C_1S_1 & C_1S_0 & B_1S_2 & B_1S_1 & B_1S_0+1 \end{vmatrix} = 0. \tag{13}$$

In the long-wavelength limit where $\omega \to 0,\ K \to 0$, the lattice sum can be decoupled as [42,43]

$$S_n = \frac{4i^{n+1}}{k_0^2\Omega}\frac{K^n}{k_0^n\left(k_0^2-K^2\right)}e^{-in\phi_K} - \frac{2^{n+3}i^{n+1}(n+1)!}{k_0^n a^{n-2}\Omega}\sum_{K_h\neq 0}\frac{J_{n+1}(K_h a)}{(K_h a)^3}e^{-in\phi_{K_h}}, \tag{14}$$

where a denotes the lattice constant, Ω is the volume of the unit cell, and $\mathbf{K}_h = (K_h, \phi_{K_h})$ is the reciprocal-lattice vector. Then in the long-wavelength limit, the lowest order lattice sums are expressed as [43,44]

$$S_0 = \frac{4i}{k_0^2\Omega}\frac{1}{k_0^2-K^2},\quad S_{\pm1} = \mp\frac{4}{k_0^2\Omega}\frac{K}{k_0\left(k_0^2-K^2\right)}e^{\mp i\phi_K},\quad S_{\pm2} = -\frac{4i}{k_0^2\Omega}\frac{K^2}{k_0^2\left(k_0^2-K^2\right)}e^{\mp 2i\phi_K}. \tag{15}$$

C. Obtaining the effective constitutive parameters

Substituting Eq. (15) into Eq. (13) and collecting together terms involving the same powers of K, the secular equation can be written as

$$PK^4k_0^{-4} + QK^2k_0^{-2} + RS = 0, \tag{16}$$

where

$$\begin{aligned} P &= (i+\Lambda A_1)(i+\Lambda B_1) - \Lambda^2C_1^2, \\ R &= (1+i\Lambda A_0)(1+i\Lambda B_0) + \Lambda^2C_0^2, \\ S &= (i-\Lambda A_1)(i-\Lambda B_1) + \Lambda^2C_1^2, \end{aligned} \tag{17}$$

with $\Lambda = 4/k_0^2\Omega$, Q is a function of the Mie coefficients and Λ (since Q is complicated and not used explicitly in the following, we do not show its explicit expression here). According to the Vieta's formulas, the two solutions to Eq. (16),K_+^2 and K_-^2, fulfill the relationship

$$K_+^2K_-^2 = k_0^4R\frac{S}{P}. \tag{18}$$

From Eq. (17), we can see that R and S/P are related to the zeroth and first order Mie coefficients, respectively. And we note that the zeroth and first order Mie coefficients are related to the monopoles and dipoles which correspond to the z and transverse components, respectively. Thus, comparing Eq. (4) with Eq. (18), we obtain

$$\varepsilon_z\mu_z - \kappa_z^2 = R,\quad \varepsilon_t\mu_t - \kappa_t^2 = \frac{S}{P}. \tag{19}$$

Substitute Eq. (17) into the first equation of Eq. (19), we can obtain the out-plane components of the effective parameters as

$$\varepsilon_z = 1+i\Lambda B_0,\quad \mu_z = 1+i\Lambda A_0,\quad \kappa_z = i\Lambda C_0. \tag{20a}$$

We can see that Eq. (20a) just reduces to the achiral form [42] when there is no chirality. The expressions for in-plane components of the effective parameters can be determined with the following considerations: according to the duality symmetry, ε_t and μ_t should be interchanged when A_1 and B_1 are interchanged; they are even functions of C_1; they can be reduced to the achiral forms of

$$\varepsilon_t = \frac{(i-\Lambda A_1)}{(i+\Lambda A_1)},\quad \mu_t = \frac{(i+\Lambda A_1)}{(i+\Lambda A_1)}, \tag{21}$$

when C_1 is zero; for κ_t, it is an odd function of C_1. With all this information, we can obtain

$$\begin{aligned} \varepsilon_t &= \frac{(i-\Lambda A_1)(i+\Lambda B_1)+\Lambda^2C_1^2}{(i+\Lambda A_1)(i+\Lambda B_1)-\Lambda^2C_1^2}, \\ \mu_t &= \frac{(i+\Lambda A_1)(i-\Lambda B_1)+\Lambda^2C_1^2}{(i+\Lambda A_1)(i+\Lambda B_1)-\Lambda^2C_1^2}, \\ \kappa_t &= \frac{-2i\Lambda C_1}{(i+\Lambda A_1)(i+\Lambda B_1)-\Lambda^2C_1^2}. \end{aligned} \tag{20b}$$

For special case of isotropic inclusions, substituting Eq. (8) into Eq. (20), then we have

$$\varepsilon_z = (\varepsilon-1)p+1,\quad \mu_z = (\mu-1)p+1,\quad \kappa_z = \kappa p, \tag{22a}$$

and

$$\begin{aligned}
\varepsilon_t &= \frac{(\varepsilon+1)(\mu+1)-\kappa^2+2p(\varepsilon-\mu)-p^2((\varepsilon-1)(\mu-1)-\kappa^2)}{(\varepsilon+1)(\mu+1)-\kappa^2+2p(1+\kappa^2-\varepsilon\mu)+p^2[(\varepsilon-1)(\mu-1)-\kappa^2]},\\
\mu_t &= \frac{(\varepsilon+1)(\mu+1)-\kappa^2-2p(\varepsilon-\mu)-p^2((\varepsilon-1)(\mu-1)-\kappa^2)}{(\varepsilon+1)(\mu+1)-\kappa^2+2p(1+\kappa^2-\varepsilon\mu)+p^2[(\varepsilon-1)(\mu-1)-\kappa^2]},\\
\kappa_t &= \frac{4p\kappa}{(\varepsilon+1)(\mu+1)-\kappa^2+2p(1+\kappa^2-\varepsilon\mu)+p^2[(\varepsilon-1)(\mu-1)-\kappa^2]},
\end{aligned} \tag{22b}$$

where $p = 4k_0^2 S/\Lambda = S/\Omega$ denotes the filling ratio and S is the geometrical cross section of the inclusion. We see that Eq. (22b) bears some resemblance to the 3D chiral Maxwell-Garnet formulas [45,46]. And when $\kappa = 0$, Eq. (22) reduces to the well-known traditional 2D Maxwell Garnett formula.

We note that Eq. (20) is more fundamental than Eq. (22) since it does not require the inclusions to be isotropic. For inclusions whose Mie coefficients fulfill $A_n = A_{-n}$, $B_n = B_{-n}$, $C_n = C_{-n}$for$n = 0, 1$, the effective constitutive parameters can be obtained using Eq. (20) once the Mie coefficients are known. Note that although the Eqs. (20) and (22) are derived starting from a periodic structure, they are valid for both regular and random lattice structures in the long-wavelength limit, since they are only related to the scattering properties of inclusions, namely the Mie coefficients, and the filling ratios.

From Eq. (22), we can obtain the following relationship:

$$\frac{\varepsilon_z-\mu_z}{\kappa_z} = \frac{\varepsilon_t-\mu_t}{\kappa_t} = \frac{\varepsilon-\mu}{\kappa}. \tag{23}$$

The same relationship has been found in 3D isotropic chiral metamaterials [46]. The identity (23) indicates that for isotropic chiral inclusions, the relation among effective constitutive parameters of the metamaterial is essentially equal to that of the inclusions. Therefore we can tune the effective constitutive parameters by adjusting the constitutive parameters of the inclusions according to Eq. (23).

Combining Eq. (13b) and Eq. (9) in Ref. [46], we can obtain a general Maxwell-Garnet form expression for both the 2D and 3D chiral metamaterials as

$$\begin{aligned}
\varepsilon_t &= \frac{[\alpha+\varepsilon-p(1-\varepsilon)][\alpha+\mu+p(1-\mu)]+\kappa^2p^2(p-1)(1+\alpha p)}{[\alpha+\varepsilon+p(1-\varepsilon)][\alpha+\mu+p(1-\mu)]-\kappa^2(p-1)^2},\\
\mu_t &= \frac{[\alpha+\varepsilon+p(1-\varepsilon)][\alpha+\mu-p(1-\mu)]+\kappa^2p^2(p-1)(1+\alpha p)}{[\alpha+\varepsilon+p(1-\varepsilon)][\alpha+\mu+p(1-\mu)]-\kappa^2(p-1)^2},\\
\kappa_t &= \frac{(\alpha+1)^2p\kappa}{[\alpha+\varepsilon+p(1-\varepsilon)][\alpha+\mu+p(1-\mu)]-\kappa^2(p-1)^2},
\end{aligned} \tag{24}$$

where $\alpha = d-1$ with d being the dimension of the system.

III. THE ELECTRO/MAGNETOSTRICTIVE TENSORS

The electrostrictive and magnetostrictive tensors describe the stiffness of constitutive parameters under stretching and shearing [47–50]. These tensors are defined as $\partial\overleftrightarrow{\varepsilon}/\partial u_{ik}$, $\partial\overleftrightarrow{\mu}/\partial u_{ik}$ and $\partial\overleftrightarrow{\kappa}/\partial u_{ik}$ for the permittivity, permeability and chirality parts, respectively. Here, $u_{ik} = (\partial u_i/\partial x_k + \partial u_k/\partial x_i)/2$ is the strain tensor with $\mathbf{u}(x)$ being the displacement vector [51]. In Fig. 2, the geometrical sketches of the stretched and sheared unit cells for square and hexagonal lattices are shown, and the strain tensor is given by $u_{xx} = 2\Delta a/a$, $u_{xy} = \Delta a/a$ for the square lattice and $u_{xx} = 2\Delta a/a$, $u_{xy} = \Delta a/(\sqrt{3}a)$ for hexagonal lattice, where Δa is an infinitesimal displacement. The electrostrictive and magnetostrictive tensors play import roles in studying the electrostriction and magnetostriction effect [50], and it has already been shown that the electrostrictive and magnetostrictive tensors are necessary for determining the optical force distribution inside metamaterials [44,52,53].

The electrostrictive and magnetostrictive tensors can be obtained by the perturbation approach using multiple scattering formulism [44]. For the lattice stretched along the x direction, the lattice sums can be expressed as [44]

$$\begin{aligned}
S_0 &= i\Lambda\frac{1}{k_0^2-K^2}(1-u_{xx}),\\
S_{\pm1} &= \mp\Lambda\frac{K}{k_0(k_0^2-K^2)}e^{\mp i\phi_K}(1-u_{xx}),\\
S_{\pm2} &= \left(-i\Lambda\frac{K^2}{k_0^2(k_0^2-K^2)}e^{\mp2i\phi_K}+i\Pi u_{xx}\right)(1-u_{xx}),
\end{aligned} \tag{25}$$

where $\Pi = 1.298\Lambda$ for the square lattice and $\Pi = 0.499\Lambda$ for the hexagonal lattice. Substituting Eq. (25) into the secular equation Eq. (13), and then we obtain $K_+^2K_-^2$ as a function of u_{xx}. Thus we could have

$$\begin{aligned}
\frac{1}{k_0^4}\frac{\partial(K_+^2K_-^2)}{\partial u_{xx}}\bigg|_{u_{xx}\to0} &= \frac{\partial}{\partial u_{xx}}\left[\left(\varepsilon_z\mu_z-\kappa_z^2\right)\left(\varepsilon_t\mu_t-\kappa_t^2\right)\right]\\
&= \left[-\Lambda(A_0+B_0)+2\Lambda\left(A_0B_0-C_0^2\right)\right]\frac{S}{P}\\
&\quad -R\frac{T}{P^2},
\end{aligned} \tag{26}$$

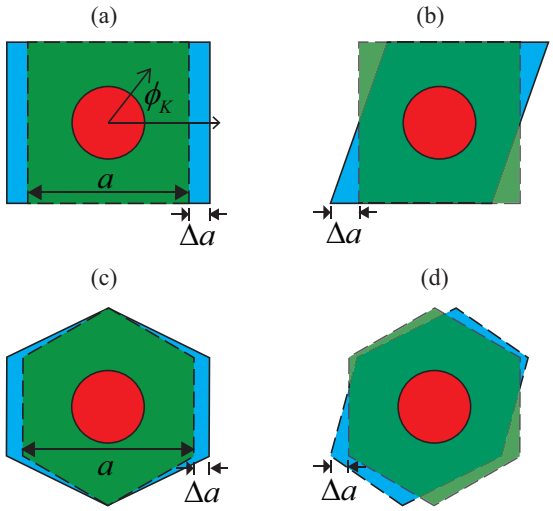

FIG. 2. The unit cell deformations used to calculate the electrostrictive and magnetostrictive tensors. The upper (lower) panels are for the square (hexagonal) lattice. [(a) and (b)] Original square lattice unit cell is shown as semitransparent green squares. The unit cell is stretched or sheared Δa in x direction, with the deformed cell shown by blue parallelograms. Here, a and ϕ_K denote the side length of cell and the direction of wave vector, respectively. [(c) and (d)] Counterparts for the hexagonal lattice.

where P, R, and S are defined in Eq. (17), and

$$\begin{aligned} T = 2\Lambda\{&\Pi B_1^2 + A_1^2[\Pi + \Lambda^2 B_1(i + 2\Pi B_1)] \\ &- iB_1(-1 + \Lambda^2 C_1^2) + 2\Pi C_1^2(1 + \Lambda^2 C_1^2) \\ &+ iA_1[1 + \Lambda^2(B_1^2 - C_1^2 + 4i\Pi B_1 C_1^2)]\}. \end{aligned} \tag{27}$$

We already know that $(\varepsilon_z\mu_z - \kappa_z^2) = R$, $(\varepsilon_t\mu_t - \kappa_t^2) = S/P$, see Eq. (19). Thus we have

$$\frac{\partial}{\partial u_{xx}}(\varepsilon_z\mu_z - \kappa_z^2) = -\Lambda(A_0 + B_0) + 2\Lambda(A_0B_0 - C_0^2) \tag{28}$$

and

$$\frac{\partial}{\partial u_{xx}}(\varepsilon_t\mu_t - \kappa_t^2) = -\frac{T}{P^2}. \tag{29}$$

According to Eq. (28) and Eq. (20a), we could easily obtain that

$$\begin{aligned} &\frac{\partial\varepsilon_z}{\partial u_{xx}} = -i\Lambda B_0 = 1 - \varepsilon_z, \quad \frac{\partial\mu_z}{\partial u_{xx}} = -i\Lambda A_0 = 1 - \mu_z, \\ &\frac{\partial\kappa_z}{\partial u_{xx}} = i\Lambda C_0 = -\kappa_z. \end{aligned} \tag{30a}$$

For the in-plane components, we write

$$\begin{aligned} \frac{\partial\varepsilon_t}{\partial u_{xx}} &= \frac{2\Lambda A_1(i + \Pi A_1)(i + \Lambda B_1)^2 - g_1C_1^2 + 2\Lambda^3\Pi C_1^4}{[(i + \Lambda A_1)(i + \Lambda B_1) - \Lambda^2 C_1^2]^2}, \\ \frac{\partial\mu_t}{\partial u_{xx}} &= \frac{2\Lambda B_1(i + \Pi B_1)(i + \Lambda A_1)^2 - g_2C_1^2 + 2\Lambda^3\Pi C_1^4}{[(i + \Lambda A_1)(i + \Lambda B_1) - \Lambda^2 C_1^2]^2}, \\ \frac{\partial\kappa_t}{\partial u_{xx}} &= \frac{f_1C_1 + f_2C_1^3}{[(i + \Lambda A_1)(i + \Lambda B_1) - \Lambda^2 C_1^2]^2}, \end{aligned} \tag{31}$$

where g_1, g_2 and f_1, f_2 are coefficients to be determined. We write $\partial\varepsilon_t/\partial u_{xx}$ and $\partial\mu_t/\partial u_{xx}$ in such forms by the consideration of three aspects. First, they should be interchanged when A_1 and B_1 are interchanged. Second, they should be even functions of C_1 (or κ). Third, they should reduce to the achiral forms

$$\frac{\partial\varepsilon_t}{\partial u_{xx}} = \frac{2\Lambda A_1(i + \Pi A_1)}{(i + \Lambda A_1)^2}, \quad \frac{\partial\mu_t}{\partial u_{xx}} = \frac{2\Lambda B_1(i + \Pi B_1)}{(i + \Lambda A_1)^2}, \tag{32}$$

when C_1 vanishes at $\kappa = 0$. For the chirality, $\partial\kappa_t/\partial u_{xx}$ should be an odd function of C_1.

Substituting Eqs. (31) and (20b) into Eq. (28), we could have

$$\begin{aligned} g_1 + g_2 &= -2\Lambda[-4\Lambda + i\Lambda(A_1^2 + B_1^2) + 2\Pi \\ &\quad + 2i\Lambda\Pi(A_1 + B_1) + 4\Lambda^2\Pi A_1B_1], \\ f_1 &= -\Lambda\{2i + 3\Pi A_1 + \Pi B_1 + \Lambda B_1[2\Pi A_1^2 - iB_1 \\ &\quad + A(3i - 2\Pi B_1)] + 2\Lambda[i\Pi A_1^2 + B_1 \\ &\quad - A_1(1 + 3i\Pi B_1)]\} - \tfrac{1}{2}(A_1 - B_1)g_1, \\ f_2 &= -2i\Lambda(-\Lambda^2 + 2\Lambda\Pi). \end{aligned} \tag{33}$$

Up to now, g_1, g_2 and f_1 are still undetermined. We use another information that Eq. (31) should be reduced to the form of the amorphous metamaterials when $\Pi = 0$. The electrostrictive and magnetostrictive tensors for amorphous metamaterials can be directly obtained according to Eq. (20b), namely,

$$\begin{aligned} \frac{\partial\varepsilon_t}{\partial u_{xx}} &= -p\frac{\partial\varepsilon_t}{\partial p} = \frac{2\Lambda[iA_1(i + \Lambda B_1)^2 + \Lambda(2 - i\Lambda B_1)C_1^2]}{[(i + \Lambda A_1)(i + \Lambda B_1) - \Lambda^2 C_1^2]^2} \\ &= \frac{2\Lambda A_1 i(i + \Lambda B_1)^2 - g_1C_1^2}{[(i + \Lambda A_1)(i + \Lambda B_1) - \Lambda^2 C_1^2]^2}\bigg|_{\Pi=0}. \end{aligned} \tag{34}$$

And considering that g_1 and g_2 should be interchanged when interchanging A_1 and B_1, we have

$$g_1 = -2\Lambda(-2\Lambda + i\Lambda^2 B_1 + \Pi + 2i\Lambda\Pi A_1 + 2\Lambda^2\Pi A_1B_1). \tag{35}$$

Substituting Eq. (35) into Eq. (31) and combining Eqs. (33) and (20b), we finally have

$$\begin{aligned} \frac{\partial\varepsilon_t}{\partial u_{xx}} &= -\frac{\varepsilon_t^2 + \kappa_t^2 - 1}{2} + \frac{(\varepsilon_t - 1)^2 + \kappa_t^2}{2}\frac{\Pi}{\Lambda}\cos 2\phi_K, \\ \frac{\partial\mu_t}{\partial u_{xx}} &= -\frac{\mu_t^2 + \kappa_t^2 - 1}{2} + \frac{(\mu_t - 1)^2 + \kappa_t^2}{2}\frac{\Pi}{\Lambda}\cos 2\phi_K, \\ \frac{\partial\varepsilon_t}{\partial u_{xx}} &= -\frac{(\varepsilon_t + \mu_t)\kappa_t}{2} + \frac{(\varepsilon_t + \mu_t - 2)\kappa_t}{2}\frac{\Pi}{\Lambda}\cos 2\phi_K. \end{aligned} \tag{30b}$$

The partial differential of the constitutive parameters with respect to u_{yy} can be directly obtained by replacing Π by $-\Pi$ [44].

For the sheared lattice, the lattice sums are [44]

$$S_0 = i\Lambda\frac{1}{k_0^2 - K^2}, \quad S_{\pm1} = \mp\Lambda\frac{K}{k_0(k_0^2 - K^2)}e^{\mp i\phi_K},$$
$$S_{\pm2} = -i\Lambda\frac{K^2}{k_0^2(k_0^2 - K^2)}e^{\mp 2i\phi_K} \mp \Xi u_{xy}, \tag{36}$$

where $\Xi = 0.596\Lambda$ for the square lattice and $\Xi = -1.0\Lambda$ for the hexagonal lattice. For the unit cell being sheared, substituting Eq. (38) into the secular equation Eq. (13), similarly we have

$$\frac{1}{k_0^4}\frac{\partial}{\partial u_{xy}}(K_+^2K_-^2)|_{u_{xy}\to 0} = \frac{\partial}{\partial u_{xy}}\left[\left(\varepsilon_z\mu_z - \kappa_z^2\right)\left(\varepsilon_t\mu_t - \kappa_t^2\right)\right] = R\frac{U}{P^2}, \tag{37}$$

with

$$U = -i\Lambda\Xi\left(A_1^2 + B_1^2 + 2\Lambda^2A_1^2B_1^2 - 4\Lambda^2A_1B_1C_1^2 + 2C_1^2 + 2\Lambda^2C_1^4\right). \tag{38}$$

Then we can easily obtain that

$$\frac{\partial}{\partial u_{xy}}\left(\varepsilon_z\mu_z - \kappa_z^2\right) = 0, \quad \frac{\partial}{\partial u_{xy}}\left(\varepsilon_t\mu_t - \kappa_t^2\right) = \frac{U}{P^2}. \tag{39}$$

We can do the same procedures as we did for the tensors of diagonal term and finally have

$$\frac{\partial\varepsilon_z}{\partial u_{xy}} = \frac{\partial\mu_z}{\partial u_{xy}} = \frac{\partial\kappa_z}{\partial u_{xy}} = 0,$$
$$\frac{\partial\varepsilon_t}{\partial u_{xy}} = -\frac{(\varepsilon_t - 1)^2 + \kappa_t^2}{2}\frac{\Xi}{\Lambda}\sin 2\phi_K,$$
$$\frac{\partial\mu_t}{\partial u_{xy}} = -\frac{(\mu_t - 1)^2 + \kappa_t^2}{2}\frac{\Xi}{\Lambda}\sin 2\phi_K,$$
$$\frac{\partial\kappa_t}{\partial u_{xy}} = -\frac{(\varepsilon_t + \mu_t - 2)\kappa_t}{2}\frac{\Xi}{\Lambda}\sin 2\phi_K, \tag{40}$$

We can see that Eqs. (30) and (40) are just reduced to the Eq. (2) in Ref. [52] when $\kappa_z = \kappa_t = 0$. We note that the validity of Eqs. (30) and (40) is not restricted to square and hexagonal lattices. For other lattice structures, we only need change the values of Π and Ξ, for example for random lattice, they are $\Pi = 0$ and $\Xi = 0$.

IV. NUMERICAL TESTING OF THE FORMULAS FOR BIANISOTROPIC METAMATERIALS COMPOSED OF ISOTROPIC INCLUSIONS

In this section, we will numerically check the validity of Eqs. (22), (30), and (40), and consider examples that the bianisotropic metamaterials are composed of isotropic cylindrical inclusions whose constitutive parameters are already known. First, we will numerically check the validity of Eq. (22). We consider a square/hexagonal lattice formed by 50 layers of cylinders ($\varepsilon = 8$, $\mu = 1$, and $\kappa = 2$) in the x direction and is periodic along the y direction. When the lattice constant a is much smaller than the wavelength, such a lattice can be regarded as an effective slap according to the EMT and the corresponding effective constitutive parameters can be obtained using Eq. (22). The validity of the effective parameters can be tested by checking the consistence between the spatially averaged lattice fields, such as the electric field and displacement field: $\bar{\mathbf{E}} = 1/\Omega\int_\Omega \mathbf{E}dS$, $\bar{\mathbf{D}} = 1/\Omega\int_\Omega \mathbf{D}dS$, and the fields in the corresponding effective medium $\mathbf{E}_e$, $\mathbf{D}_e$, as in the long-wavelength limit these two should be equal [54]. To do this, we consider a H_z polarized plane wave obliquely incident on the lattices, as shown in the insets of Fig. 3, and calculate the spatially averaged lattice fields using a commercial finite-element-method package COMSOL [55]. The electric field and displacement field along the x direction inside the corresponding effective medium are also numerically computed. We can see that for both square [Fig. 3(a)] and hexagonal lattices [Fig. 3(b)], the spatially averaged lattice fields (symbols) are in accordance with the fields in effective mediums (lines). Such consistence also exists for the magnetic field. This indicates that our formulas Eq. (22) can correctly determine the effective constitutive parameters for this kind of bianisotropic metamaterials.

Another way to test the validity of Eq. (22) is by checking the consistency of the effective refractive indices of the metamaterials and those of the corresponding effective mediums. The former can be numerically determined from the slopes

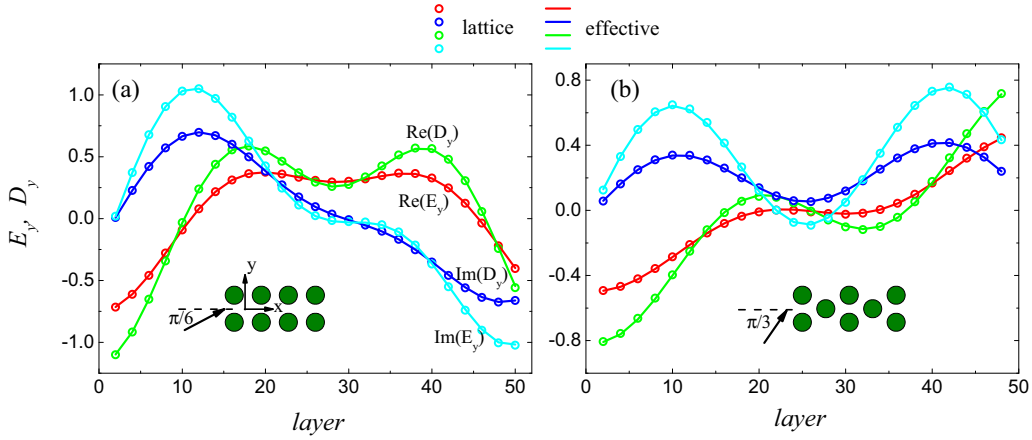

FIG. 3. The spatially averaged electric field and displacement field of each layer inside the metamaterials with (a) the square and (b) hexagonal lattices are noted by the circles. The electric field and displacement field along the x direction in each corresponding effective continuous medium under same incidence are shown by lines. The inclusions of the metamaterials possess $\varepsilon = 8$, $\mu = 1$, $\kappa = 2$, and $r_0 = 0.3a$.

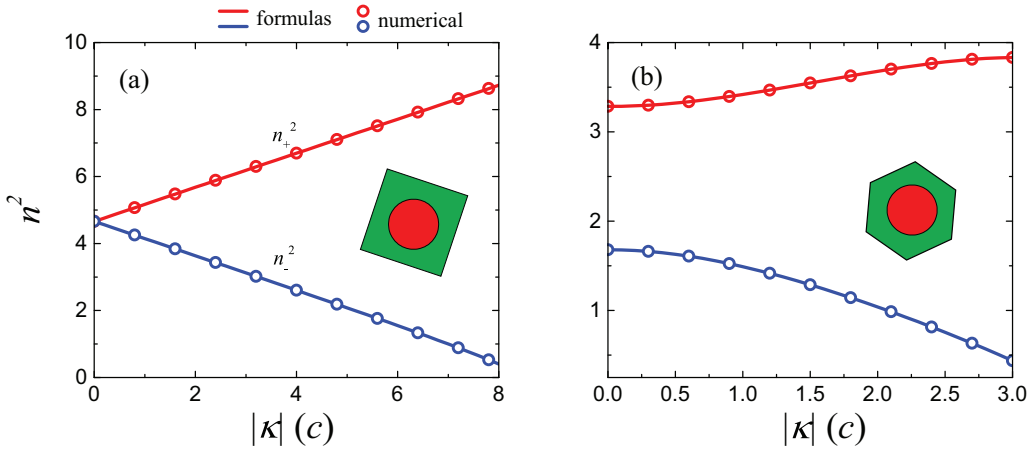

FIG. 4. Comparison between the refractive indices obtained from the formulas and those from numerical calculations for both (a) the square and (b) hexagonal lattice structures. The horizontal axis denotes the absolute chirality of the inclusions. For the square lattice, the inclusions possess $\varepsilon = \mu = 8$, and for hexagonal lattice the inclusions possess $\varepsilon = 8$ and $\mu = 1$. The cylinders have radius $r_0 = 0.3a$.

of photonic band dispersion in the limit $\omega \to 0$ and $k \to 0$. The latter can simply be obtained using Eq. (3) where the effective constitutive parameters used are obtained according to Eq. (22). Note that two refractive indices $n_+ = K_+/k_0$ and $n_- = K_-/k_0$ are considered here, corresponding to two eigenmodes. The comparison results as functions of chirality are shown in Fig. 4. We set $\varepsilon = \mu = 8$ for the inclusions of the square lattice and $\varepsilon = 8$, $\mu = 1$ for the inclusions of the hexagonal lattice. It is seen that in both cases the numerical results (symbols) match the analytical results (lines) very well, again confirming the validity of the derived analytical formulas for the effective constitutive parameters.

The validity of the derived electrostrictive and magnetostrictive tensors in Eqs. (30) and (40) are tested by comparing them with numerical simulation results, which are obtained using the eigenfields and the band dispersions combined with finite-differences method (see the details in Appendix A). The comparison results for both the square and hexagonal lattices

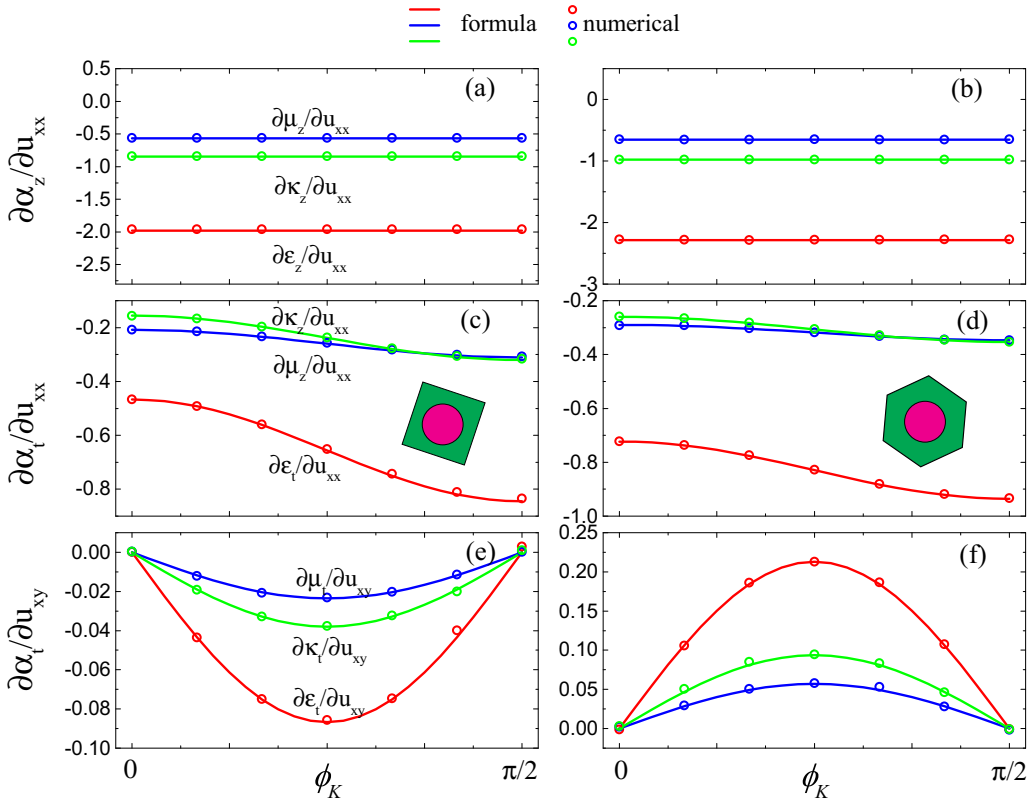

FIG. 5. Comparison between tensor components obtained from analytic formulas and those from numerical calculations for both square and hexagonal lattice structures. Results as functions of the direction of Bloch vector ϕ_K obtained from the formulas and numerical calculations are shown by lines and circles, respectively. α denotes ε, μ, or κ. The inclusions of the metamaterials possess constitutive parameters $\varepsilon = 8$, $\mu = 3$, $\kappa = 3$, and radius $r_0 = 0.3a$.

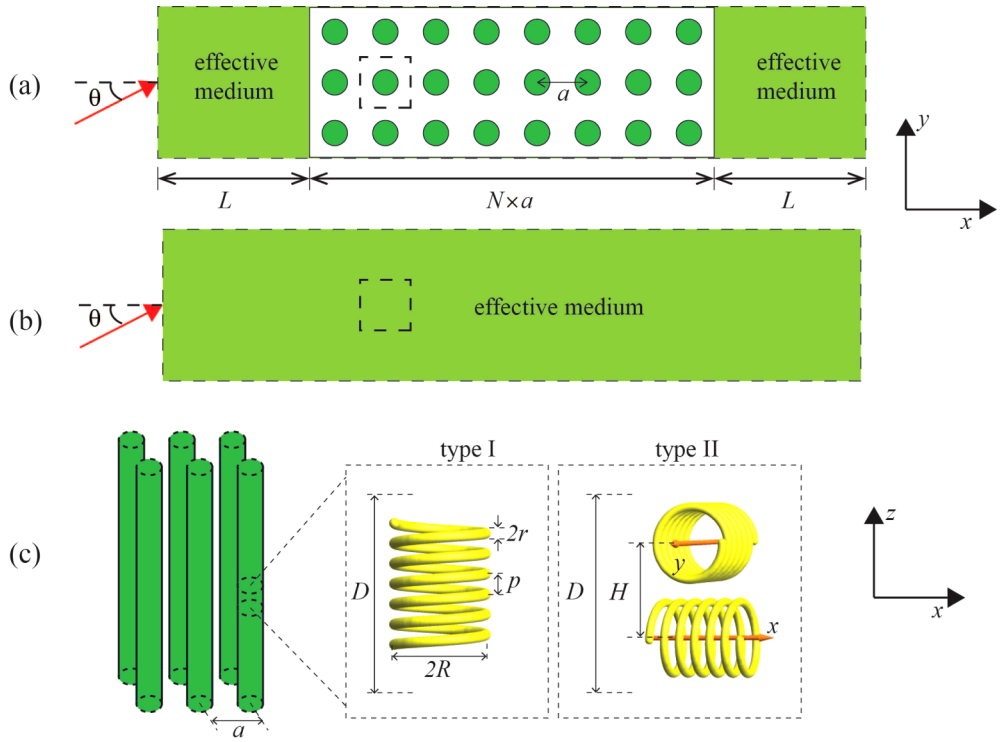

FIG. 6. (a) The sandwiched metamaterial slab is composed of artificial chiral cylinders arranged into a square lattice (lattice constant a) in the xy plane. These artificial cylinders are formed by a chain of helices as shown in panel (c). There are N layers in the x direction periodic along the y direction. The incident wave vector (red arrow) forms an angle θ with x axis. (b) The corresponding effective homogenous medium. The black dashed line in (a) and (b) marks the boundary of a unit cell, used in electromagnetic stress tensor integrations. (c) There are two types of artificial chiral cylinders that consist of identical gold helixes periodically arranged into a chain along z direction. The unit cells of the chains for the two types are shown in the dashed line boxes. Type-I structure has an out-of-plane chirality component κ_z while type II has an in-plane chirality component κ_t. The period of the unit cell along z direction is $D = 2H = 1.2\,\mu$m. Each helix contains 6 pitches and we set the geometrical parameters of the helix as $r = 15$ nm, $R = 200$ nm, and $p = 100$ nm.

are shown in Fig. 5. The constitutive parameters of the cylinders are $\varepsilon = 8$, $\mu = 3$, and $\kappa = 3$, and the radius is $r_0 = 0.3a$. The tensor components $\partial\varepsilon_z/\partial u_{xy}$, $\partial\mu_z/\partial u_{xy}$, and $\partial\kappa_z/\partial u_{xy}$ are zero and not shown here. We can see clearly that the electrostrictive and magnetostrictive tensors obtained from numerical calculations (circles) are identical to those calculated using the formulas (lines). Since the results obtained using the numerical method correspond to the real system, the consistency indicates that our formulas Eqs. (30) and (40) can correctly produce the elecrto/magnetostrictive tensors.

For the inclusions which are not isotropic, Eq. (22) is no longer applicable. However, we can use Eq. (20) as well as Eqs. (30) and (40) to calculate the effective constitutive parameters and the electro/magnetostrictive tensors. Equations. (20), (30), and (40) are valid once the two conditions are met: 1) the Mie coefficients of the inclusions fulfill $A_n = A_{-n}$, $B_n = B_{-n}$, and $C_n = C_{-n}$ for $n = 0, 1; 2$) the long-wavelength limit is good. We find that the formulas can still produce rather accurate results in configurations where the two conditions are not exactly fulfilled, as we will show in the following section.

V. BIANISOTROPIC METAMATERIALS REALIZED BY HELICAL STRUCTURES

Because chirality in natural materials is usually very weak, bianisotropic metamaterials are frequently fabricated using man-made inclusions with complex underlying structures possessing strong magnetoelectric coupling using resonance. Examples of resonating structures include metallic split rings [19–21,27,28,30], gammadions [22,29,31], and helices [16,18]. Here, we use two kinds of helix chains which are labeled as type I and II to form the artificial chiral inclusions, as shown in Fig. 6(c). The type-I inclusion consists of a chain of helices with axis along the z direction, while the type II consists of a chain of helices with orthogonal axes along x and y directions, respectively. The helix chains are along z direction and have the same period D. Therefore the bianisotropic metamaterials composed of type-I and type-II inclusions possess out-of-plane chirality κ_z and in-plane chirality κ_t, respectively. Each helix we used has minor radius $r = 15$ nm, major radius $R = 200$ nm and contains 6 pitches with pitch length $p = 100$ nm. The helices are made of gold whose relative permittivity is described by the Drude model $\varepsilon_{\rm Au} = 1 - \omega_p^2/(\omega^2 + i\omega\omega_\tau)$ with plasma frequency $\omega_p = 1.36 \times 10^{16}\,{\rm s}^{-1}$ and damping frequency $\omega_\tau = 4.084 \times 10^{13}\,{\rm s}^{-1}$. As the pitch length p is much smaller than the major radius R, the helix is almost rotational invariant about its axis. As such, the Mie coefficients of the type-I and -II cylinders fulfill $A_n \approx A_{-n}$, $B_n \approx B_{-n}$, and $C_n \approx C_{-n}$ (verified by the numerical calculations) which is one of the condition that the effective parameters of the metamaterials composed of these cylinders can be calculated using Eq. (20). And also, the lattice constant of the metamaterial is set to

be $a = 1\,\mu$m, which is much smaller than the wavelength $\lambda = 21.43\,\mu$m of the incident wave (corresponding to the resonant frequency $f = 14\,$THz), and the other necessary condition, namely the long-wavelength limit approximation, is met. Therefore, we can use Eq. (20) to calculate the effective constitutive parameters for the bianisotropic metamaterials we considered here. For the inclusions with helical structures, the Mie coefficients can no longer be obtained directly from Eq. (8). But we can acquire the Mie coefficients numerically according to the scattering fields of a single inclusion. The detail of the numerical method will be shown in the following section.

A. Numerically obtaining the Mie coefficients of the artificial cylinders

The Mie coefficients of the artificial chiral cylinder can be determined according to the scattering fields $\mathbf{E}_s$ and $\mathbf{H}_s$ of the cylinder in the far field region. Since the scattering fields can be expanded in terms of a complete orthogonal set, namely the vector cylindrical wave functions $\mathbf{M}_n^{(3)}$ and $\mathbf{N}_n^{(3)}$, see Eq. (5), the scattering coefficients can be obtained by

$$a_n = \frac{1}{2\pi H_{n-1}^{(1)}(k_0 r) H_{n+1}^{(1)}(k_0 r)} \int_0^{2\pi} \mathbf{E}_s \cdot \left[\mathbf{M}_n^{(3)}(k_0, \mathbf{r})\right]^* d\phi,$$

$$b_n = -\frac{1}{2\pi \left[H_n^{(1)}(k_0 r)\right]^2} \int_0^{2\pi} \mathbf{E}_s \cdot \left[\mathbf{N}_n^{(3)}(k_0, \mathbf{r})\right]^* d\phi, \qquad (41)$$

where we defined

$$\left[\mathbf{M}_n^{(3)}(k, \mathbf{r})\right]^* = \left[\frac{in}{kr} H_n^{(1)}(kr)\mathbf{e}_r - H_n^{(1)\prime}(kr)\mathbf{e}_\phi\right] e^{-in\phi},$$

$$\left[\mathbf{N}_n^{(3)}(k, \mathbf{r})\right]^* = H_n^{(1)}(kr) e^{-in\phi} \mathbf{e}_z.$$

The scattering coefficients can also be obtained according to the magnetic scattering field as

$$a_n = \frac{1}{i} \frac{1}{2\pi \left[H_n^{(1)}(k_0 r)\right]^2} \int_0^{2\pi} \mathbf{H}_s \cdot \left[\mathbf{N}_n^{(3)}(k_0, \mathbf{r})\right]^* d\phi,$$

$$b_n = \frac{i}{2\pi H_{n-1}^{(1)}(k_0 r) H_{n+1}^{(1)}(k_0 r)} \int_0^{2\pi} \mathbf{H}_s \cdot \left[\mathbf{M}_n^{(3)}(k_0, \mathbf{r})\right]^* d\phi. \qquad (42)$$

Equations (41) and (42) produce the same results in principle. And then we can further obtain the Mie coefficients according to the relations Eq. (6) once the expansion coefficients for the incident field p_n, q_n are known.

For H_z-polarized plane wave propagating along the x direction, we have $p_n = -i^n$, $q_n = 0$, and for E_z-polarized plane wave propagating along the x direction, we have $p_n = 0$, $q_n = i^n$. As a result, we can obtain two sets of scattering coefficients after solving the scattering fields in the far field region and applying Eqs. (41) or (42) when the artificial cylinder illuminated by a H_z and a E_z-polarized plane wave, respectively. And then we further obtain the Mie coefficients using the identity Eq. (6). In the simulations, we use the commercial software COMSOL [55] to solve the scattering fields of a single artificial cylinder. We found that the Mie coefficients of the type I and type II inclusions satisfy $A_n \approx A_{-n}$, $B_n \approx B_{-n}$, and $C_n \approx C_{-n}$ for $n = 0, 1$. This is one necessary condition that the effective parameters of the metamaterials composed of these cylinders can be calculated using Eq. (20).

In our method, the retrieval of the Mie coefficients only needs to be done once if the metamaterials with different lattice constants and symmetries are made using the same inclusions. This is an advantage comparing with conventional parameter retrieval methods [27–31], which requires the repetition of the retrieval procudure when the lattice constant or symmetry changes. And we only need to calculate the scattering of a single inclusion but not the reflectance and transmittance of a lattice of inclusions, which is obviously more efficient. In addition, after obtaining the effective constitutive parameters, we can calculate the electrostrictive and magnetostrictive tensors directly using Eqs. (30) and (40), avoiding the numerical error accumulation resulting from taking numerical derivatives using finite difference procedures.

B. Numerically testing the results produced by Eqs. (20), (30), and (40)

To test whether the effective constitutive parameters calculated using Eq. (22) are correct, we consider the configuration shown in Fig. 6(a), with a plane wave incident obliquely on the bianisotropic metamaterial slab with a square lattice structure, which has N layers along the x direction and is periodic along the y direction. In the long-wavelength limit, the metamaterial can be treated as an effective homogenous medium. The metamaterial, which is sandwiched by two layers of effective medium of the same type, should correspond to the effective medium slab shown in Fig. 6(b). We note that introducing the two layers of effective medium in Fig. 6(a) helps to reduce the boundary effect, which does not affect the physics discussed here.

We first consider bianisotropic metamaterial composing of an array of type I chiral cylinders, where the helices are right-handed. The quality of the effective constitutive parameters calculated by Eq. (22) can be checked by comparing the spatially averaged lattice fields $(1/\Omega \int_\Omega \mathbf{E} d\Omega, 1/\Omega \int_\Omega \mathbf{H} d\Omega)$ and the effective fields $(\mathbf{E}_e, \mathbf{H}_e)$ in the corresponding effective medium, just as we did in previous section. With no loss of generality, we consider a H_z polarized plane wave incident from the left-hand side at an angle of $\theta = \pi/6$, and the comparison for the y component fields is shown in Fig. 11(a). We can see that the spatially averaged lattice fields (circles) match the effective fields (lines) well. So the effective constitutive parameters provide an accurate description of the fields inside the metamaterial. We next consider the bianisotropic metamaterial composed of type-II cylinders and assume the same lattice constant and incident wave as in type I. Figure 12(a) shows that the spatially averaged lattice fields and the effective fields in the corresponding effective medium are consistent with each other, indicating that the effective constitutive parameters are correctly obtained. For the type-II metamaterials, we also considered the case that each helix possesses a high dielectric core with relative permittivity $\varepsilon_c = 12.5$, as shown in the inset of Fig. 12(c), and considered a E_z polarized plane wave incident with incident angle $\theta = \pi/3$. The results are shown in Fig. 12(c), and we can see the consistency between the spatially averaged lattice fields and the fields inside the effective medium at the resonant frequency $f = 10.6\,$THz.

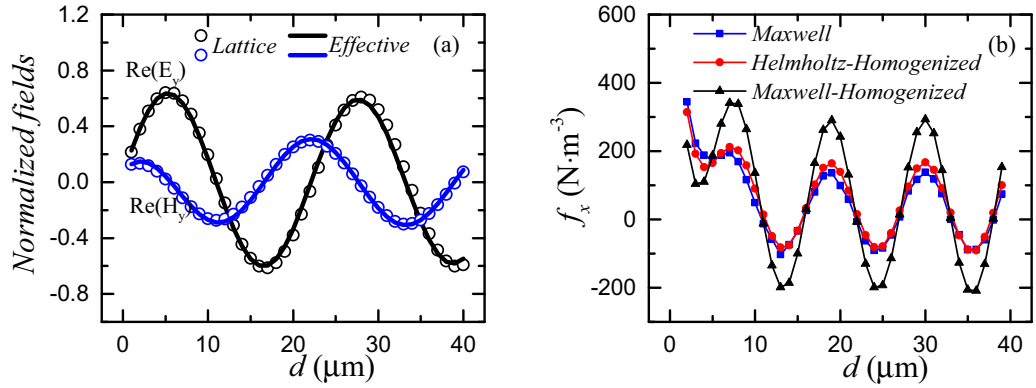

FIG. 7. (a) Comparison of the spatially averaged EM fields inside the metamaterial using full wave simulations (circles) and the effective fields in corresponding effective medium (lines) for type-I structure. The field intensity is normalized by the incident fields. (b) Optical force densities calculated using different approaches. The incident plane wave is H_z-polarized with an amplitude of $E_0 = 10^5 V/m$ wavelength in vacuum $\lambda = 21.43\,\mu$m. Other parameters are $N = 40$, $a = 1\,\mu$m, $L = 0.2\,\mu$m, and $\theta = \pi/6$. The effective constitutive parameters for the metamaterials are given by Eq. (20) as $\varepsilon_z = 0.666 + 1.05i$, $\mu_z = 0.928 + 0.140i$, $\kappa_z = -0.160 + 0.392i$, $\varepsilon_t = 1.21$, $\mu_t = 1.00$, and $\kappa_t = 0$.

We also used the numerical calculation results to test the validity of Eq. (30). The numerical calculation is based on analyzing the eigenfields and the band dispersions combined with finite-differences method (see details in Appendix A). However, because the lattice fields contain strong surface plasmon fields and the system is a three-dimensional one, too much memory is required to ensure the dispersion relations and the fields are calculated accurately enough for applying the finite difference method. As a consequence, we first treated the helix chain as an effective cylinder with

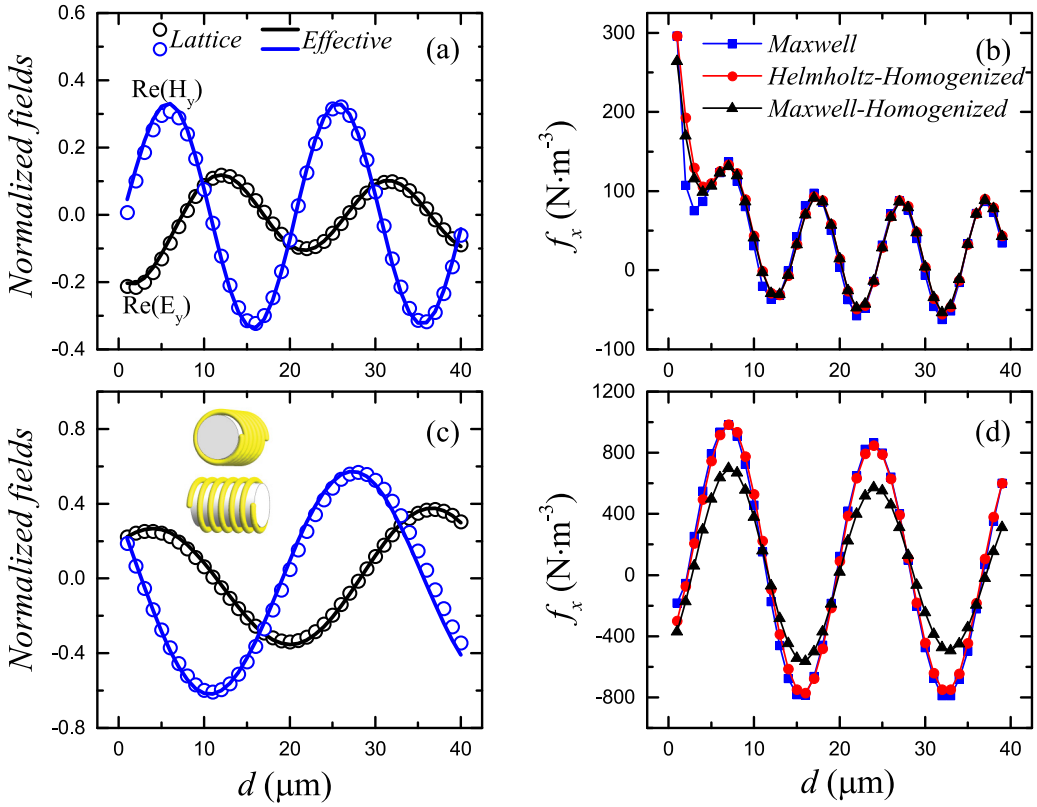

FIG. 8. (a) Comparison of the spatially averaged EM fields inside the metamaterial (circles) and the effective fields in corresponding effective medium (lines) for type-II cylinders. (b) Optical force density evaluated using different approaches. (c) Comparison of the spatially averaged EM fields inside the metamaterial formed of helices with a high dielectric ($\varepsilon_c = 12.5$) cylinder core. The dielectric core (shown by the inset) has height $H' = 0.6\,\mu$m and radius $R' = 170$ nm. (d) Optical force density evaluated using different approaches for the metamaterial formed of helices with dielectric core. For (a) and (b), the incident wave is H_z-polarized with $\lambda = 21.43\,\mu$m and $\theta = \pi/6$, and the effective parameters are $\varepsilon_z = 1.47$, $\mu_z = 1.00$, $\kappa_z = 0$, $\varepsilon_t = 0.751 + 0.835i$, $\mu_t = 0.933 + 0.129i$, and $\kappa_t = -0.173 + 0.327i$. For (c) and (d), the incident wave is E_z-polarized with $\lambda = 28.28\,\mu$m and $\theta = \pi/3$, and the effective parameters are $\varepsilon_z = 1.49$, $\mu_z = 1.0$, $\kappa_z = 0$, $\varepsilon_t = 1.26 + 0.42i$, $\mu_t = 0.969 + 0.116i$, and $\kappa_t = -0.062 + 0.220i$. Other parameters are $N = 40$, $a = 1\,\mu$m, $L = 1\,\mu$m, and $E_0 = 10^5$V/m.

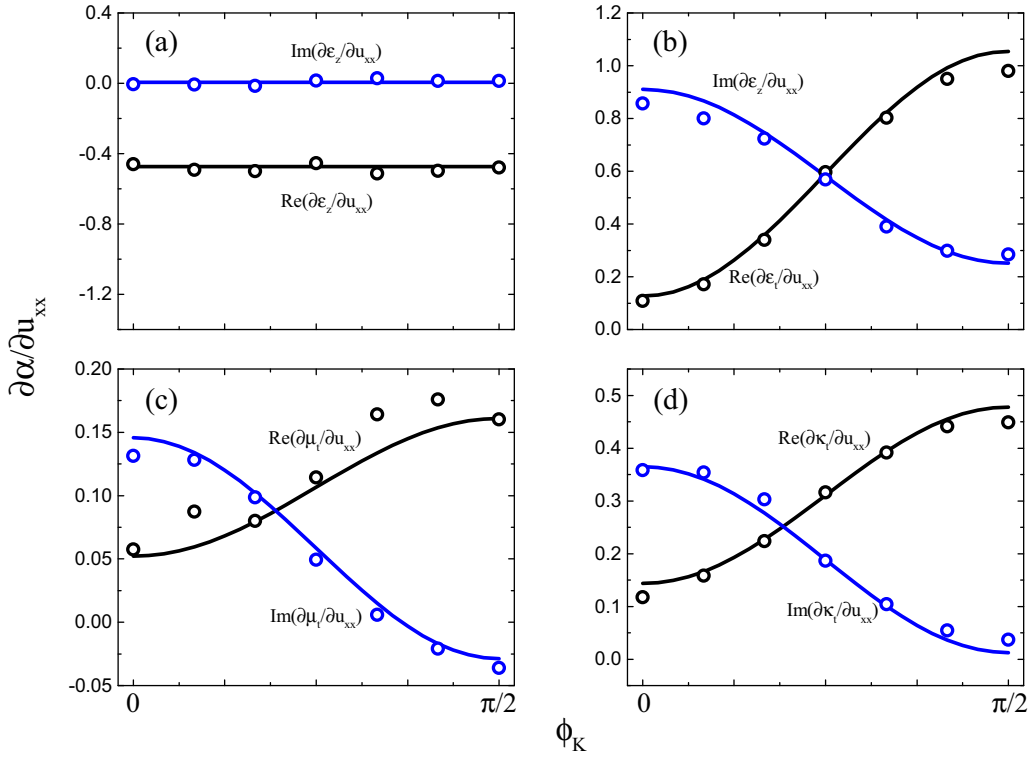

FIG. 9. For metamaterials composed by type-I chiral cylinders, the comparison between tensor components obtained from formulas (lines) and those from numerical calculations (circles). Results as functions of the direction of Bloch vector ϕ_K obtained from the formulas and numerical calculations are shown by lines and circles, respectively.

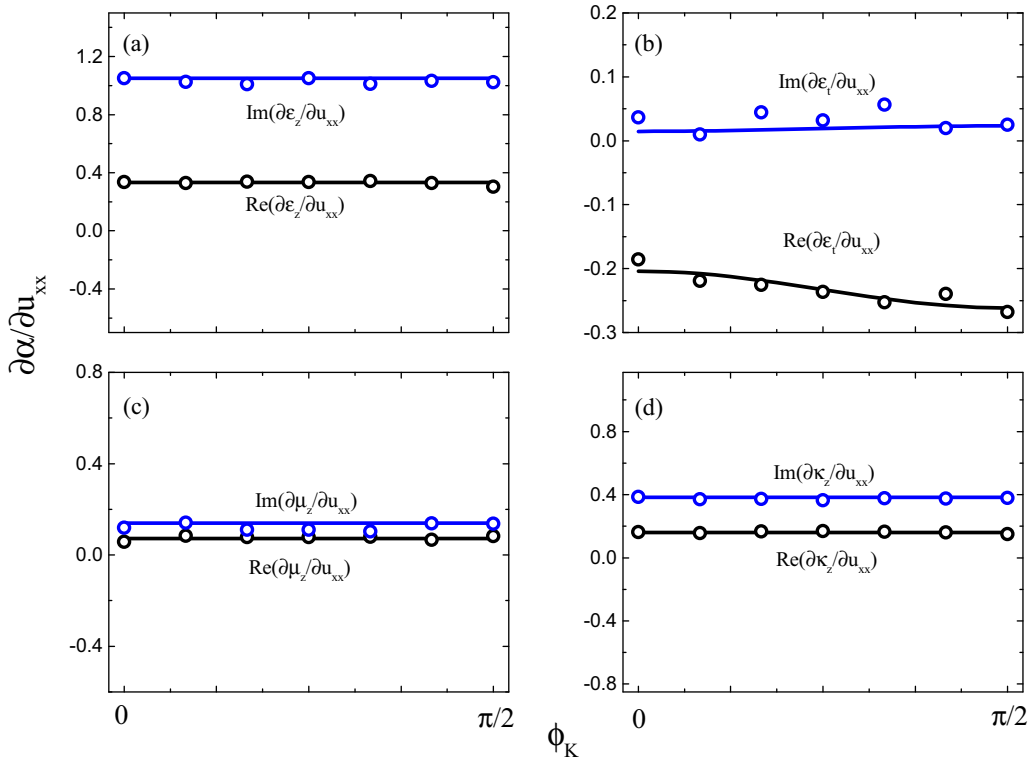

FIG. 10. For metamaterials composed by type-II chiral cylinders, the comparison between tensor components obtained from formulas (lines) and those from numerical calculations (circles). Results as functions of the direction of Bloch vector ϕ_K obtained from the formulas and numerical calculations are shown by lines and circles, respectively.

a radius $r_{\text{eff}} = 600\,\text{nm}[\Lambda = 4/(k_0^2\pi r_{\text{eff}}^2)]$ and calculated its effective constitutive parameters for the effective cylinder using Eq. (20). We then applied the numerical method to calculate the electrostrictive and magnetostrictive tensors for the bianisotropic metamaterials composed of these effective bianisotropic cylinders, just as we did in Sec. IV. As the materials are lossy, we used the weak-form-PDE module in COMSOL [55] for non-Hermitian systems to calculate the complex Bloch k bands (the frequency is real while the Bloch k is complex) and the eigenfields, see the method detailed in Appendix B. The electrostritive and magnetostrictive tensors are obtained from the formulas by substituting the effective constitutive parameters, which are shown in captions of Figs. 7 and 8, into Eq. (30). Comparisons between the two calculations for type-I and type-II bianisotropic metamaterials are shown in Figs. 9 and 10, respectively, and the results calculated by the formulas and the numerical method are shown by the lines and circles, respectively. We can see that the results obtained using analytic formulas are nearly the same with the numerical results for every ϕ_K. We note that the discrepancy between the lines (analytic formula) and circles (numerical results) in Figs. 9 and 10 is slightly bigger than those shown in Fig. 5. The discrepancy can be made smaller if we made the helix unit and the lattice constant smaller (but the chirality will be weaker).

VI. ELECTROMAGNETIC STRESS TENSOR FOR BIANISOTROPIC MEDIUM

Electromagnetic stress tensors can be obtained using the virtual work principle under the quasi static limit [51,56]. Conventional stress tensors are formulated for achiral medium. Here we derive an extended form of the stress tensor that works for the bianisotropic medium whose constitutive parameters given by Eq. (1).

Consider a small square area inside the bianisotropic medium with volume $ds = a \times b$, as shown in Fig. 11. As the EM fields inside this area are almost constant in the long wavelength limit, the time-averaged total EM energy for this area is given by $W = -\frac{1}{4}\text{Re}(\mathbf{E}\cdot\mathbf{D}^* + \mathbf{H}\cdot\mathbf{B}^*)ab$. If we subject one of the boundaries to a virtual translation over an infinitesimal distance $\boldsymbol{\xi}$, then the variance of the total electric energy δW should be just equal to the work done by the boundary force $\sum T_{ik}\xi_i n_k b$, where T_{ik} is the surface stress tensor and $\mathbf{n}$ is the unit normal vector of the boundary. Hence we have

$$\sum T_{ik}\xi_i n_k b = \delta W = \delta W_s + \delta W_f + \delta W_p, \tag{43}$$

where the variation of total EM energy δW consists of three parts which are due to the variations of total volume of the area, EM fields and constitutive parameters, respectively, and

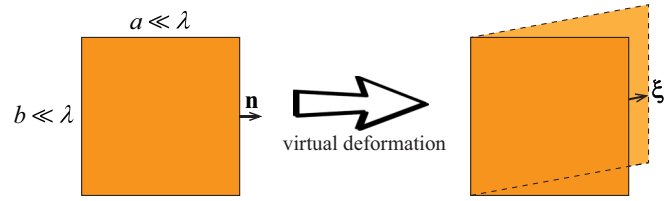

FIG. 11. For a very small area dS, the total electric energy of this area is $-1/4\text{Re}(\mathbf{E}\cdot\mathbf{D}^*+\mathbf{H}\cdot\mathbf{B}^*)dS$. If we subject one of the boundaries to a virtual translation over an infinitesimal distance $\boldsymbol{\xi}$, then the variance of the total electric energy should be just equal to the work done by the electric component of the boundary force $T_{ik}\xi_i n_k b$, where T_{ik} is the surface stress tensor and $\boldsymbol{n}$ is the normal vector of the boundary.

they are given by

$$\begin{aligned}\delta W_s &= -\frac{1}{4}\text{Re}(\mathbf{E}\cdot\mathbf{D}^* + \mathbf{H}\cdot\mathbf{B}^*)b\mathbf{n}\cdot\boldsymbol{\xi} \\ &= -\frac{1}{4}\text{Re}(\mathbf{E}\cdot\mathbf{D}^* + \mathbf{H}\cdot\mathbf{B}^*)b\sum\delta_{ik}\xi_i n_k, \end{aligned}\tag{44a}$$

$$\begin{aligned}\delta W_f &= \frac{\partial}{\partial\mathbf{E}}\left[-\frac{1}{4}\text{Re}(\mathbf{E}\cdot\mathbf{D}^* + \mathbf{H}\cdot\mathbf{B}^*)\right]\cdot\delta\mathbf{E}ab \\ &\quad + \frac{\partial}{\partial\mathbf{H}}\left[-\frac{1}{4}\text{Re}(\mathbf{E}\cdot\mathbf{D}^* + \mathbf{H}\cdot\mathbf{B}^*)\right]\cdot\delta\mathbf{H}ab, \end{aligned}\tag{44b}$$

$$\delta W_p = \sum\frac{\partial}{\partial\eta}\left[-\frac{1}{4}\text{Re}(\mathbf{E}\cdot\mathbf{D}^* + \mathbf{H}\cdot\mathbf{B}^*)\right]\cdot\delta\eta ab, \tag{44c}$$

where δ_{ik} is Kronecher delta function, $\eta = \varepsilon_t, \varepsilon_z, \mu_t, \mu_z, \kappa_t, \kappa_z$ are constitutive parameters. Note that the potential of each point on the boundary remains invariant during the deformation [51], namely $\mathbf{E}'\cdot\mathbf{n}a + \mathbf{E}'\cdot\boldsymbol{\xi} = \mathbf{E}\cdot\mathbf{n}a$ and $\mathbf{E}'\times\mathbf{n}b = \mathbf{E}\times\mathbf{n}b$, then we have

$$\delta\mathbf{E} = \mathbf{E}' - \mathbf{E} = -\mathbf{n}\frac{\mathbf{E}\cdot\boldsymbol{\xi}}{a}, \quad \delta\mathbf{H} = \mathbf{H}' - \mathbf{H} = -\mathbf{n}\frac{\mathbf{H}\cdot\boldsymbol{\xi}}{a}. \tag{45}$$

Substituting the relations into Eq. (44b), we have

$$\begin{aligned}\delta W_f &= \frac{1}{2}\text{Re}(\mathbf{n}\cdot\mathbf{D}^*)(\mathbf{E}\cdot\boldsymbol{\xi})b + \frac{1}{2}\text{Re}(\mathbf{n}\cdot\mathbf{B}^*)(\mathbf{H}\cdot\boldsymbol{\xi})b \\ &= \frac{1}{2}\sum\text{Re}(E_i D_k^* + H_i B_k^*)\xi_i n_k. \end{aligned}\tag{46}$$

The constitutive parameters are related to the strain tensors,

$$\delta\varepsilon_j = \frac{\partial\varepsilon_j}{\partial u_{ik}}u_{ik}, \quad \delta\mu_j = \frac{\partial\mu_j}{\partial u_{ik}}u_{ik}, \quad \delta\kappa_j = \frac{\partial\kappa_j}{\partial u_{ik}}u_{ik}.$$

with the strain tensors given by [51]

$$u_{ik} = \frac{1}{2}\left(\frac{\partial u_i}{\partial x_k} + \frac{\partial u_k}{\partial x_j}\right) = \frac{1}{2a}(\xi_i n_k + \xi_k n_i).$$

Then Eq. (33c) is reduced to

$$\begin{aligned}\delta W_p = -\frac{1}{4}\text{Re}\Bigg[&\varepsilon_0\left(\frac{\partial\varepsilon_t}{\partial u_{ik}}|\mathbf{E}_t|^2 + \frac{\partial\varepsilon_z}{\partial u_{ik}}|E_z|^2\right) + \mu_0\left(\frac{\partial\mu_t}{\partial u_{ik}}|\mathbf{H}_t|^2 + \frac{\partial\mu_z}{\partial u_{ik}}|H_z|^2\right) \\ &+ \frac{2}{c}\text{Im}(E_x H_x^* + E_y H_y^*)\frac{\partial\kappa_t}{\partial u_{ik}} + \frac{2}{c}\text{Im}(E_z H_z^*)\frac{\partial\kappa_z}{\partial u_{ik}}\Bigg], \end{aligned}\tag{47}$$

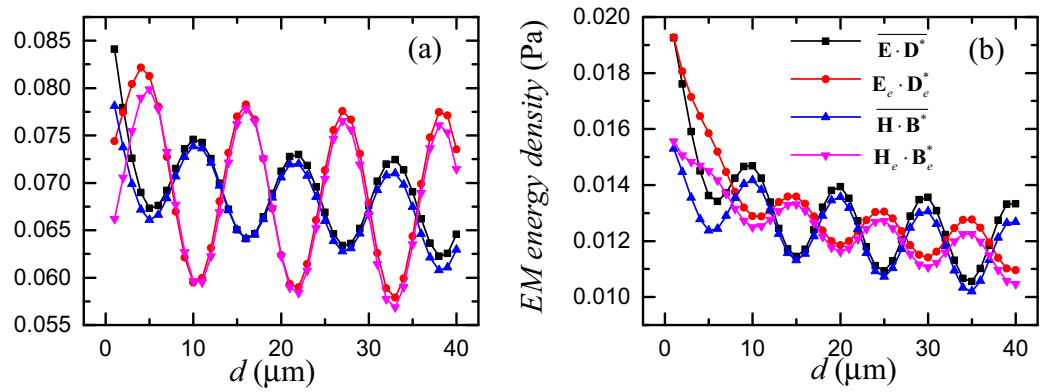

FIG. 12. Comparison between the spatially averaged EM energy density inside bianisotropic metamaterials using full wave simulations and the EM energy density in the corresponding effective medium. (a) The parameters used are the same with those in Fig. 7. (b) The parameters used are the same with those in Figs. 8(a) and 8(b).

where $\mathbf{E}_t = (E_x, E_y)$, $\mathbf{H}_t = (H_x, H_y)$ are EM fields in the xy plane. Combining Eqs. (43), (44a), (46), and (47), we can then generalize the extended Helmholtz stress tensor for the bianisotropic medium as

$$T_{ik} = \mathrm{Re}\left\{ \frac{E_i D_k^* + H_i B_k^*}{2} - \frac{1}{4}(\mathbf{E}\cdot\mathbf{D}^* + \mathbf{H}\cdot\mathbf{B}^*)\delta_{ik} - \frac{\varepsilon_0}{4}\sum_j \frac{\partial \varepsilon_j}{\partial u_{ik}}|E_j|^2 - \frac{\mu_0}{4}\sum_j \frac{\partial \mu_j}{\partial u_{ik}}|H_j|^2 + \frac{1}{2c}\sum_j \frac{\partial \kappa_j}{\partial u_{ik}}\mathrm{Im}(E_j H_j^*)\right\}. \quad (48)$$

We call Eq. (48) the extended Helmholtz stress tensor here because it is an extended form of traditional Helmholtz stress tensor [51,56] that only works for achiral medium, and Eq. (48) will reduce to the traditional Helmholtz stress tensor when all the chirality terms vanish. If we ignore the electro/magnetostrictive terms of Eq. (48), we will obtain the Minkowski stress tensor. We also see that the Maxwell stress tensor is the form of Eq. (48) in vacuum. Equation (48) is derived by applying virtual work principle based on free energy formulation of the EM problem. Therefore, when it is for the metamaterial medium, it requires that the EM energy density, i.e., $-1/4\mathrm{Re}(\mathbf{E}_e\cdot\mathbf{D}_e^* + \mathbf{H}_e\cdot\mathbf{B}_e^*)$, of macroscopic effective medium must be equal to that of the microscopic metamaterial lattice. We proved in the Appendix C that such a relationship holds in the long-wavelength limit. For bianisotropic metamaterials with real micro-structures, such as type-I and II bianisotropic metamaterials, we calculated the spatially averaged energy densities inside the metamaterial using full wave simulations and the energy densities inside the corresponding effective mediums and we show the results in Fig. 12. We note that the agreement between the microscopic spatially averaged and effective medium energy densities is not good near the boundaries. It is expected since EMT description will fail close to the boundaries. The spatially averaged energy density is almost but not exactly identical to the corresponding energy density inside the effective medium, this is because the lattice constant in the real structure is not that small compared with the wavelength.

VII. OPTICAL FORCE DENSITY INSIDE BIANISOTROPIC METAMATERIALS

In this section, we studied the optical force density inside the type-I and II bianisotropic metamaterials. The configurations are the same with those considered in Sec. V. We did three types of calculations. For the first type, the total force acting on each chiral cylinder is calculated by integrating the Maxwell stress tensor over a boundary that encloses the cylinder [such as the dashed square in Fig. 6(a)]. The fields are obtained using full wave simulations. Dividing this force by the unit cell area gives the optical force density. The force density determined in this way is by definition correct because the cylinders are immersed in air and the unit cell area is small enough. For the second type calculation, we integrate the extended Helmholtz stress tensor over the boundary that encloses the same region in the corresponding effective medium [such as the dashed square in Fig. 6(b)], using macroscopic effective fields and effective parameters. The obtained force divided by the same area corresponds to the optical force density within the effective medium framework. For the third type, we redid the effective medium calculation using the Maxwell stress tensor instead of the extended Helmholtz stress tensor.

For type-I bianisotropic metamaterials, the results produced by the three different approaches are summarized in Fig. 11(b) as blue, red, and black symbol lines, respectively. We see that the extended Helmholtz stress tensor produces results that agree well with the microscopic lattice results, while the Maxwell stress tensor fails to do so. For type-II bianisotropic metamaterials, Fig. 12(b) shows the optical force density inside the metamaterial obtained using the Maxwell stress tensor under the full wave simulations and the optical force densities inside the corresponding effective medium obtained using both the extended Helmholtz and Maxwell stress tensors within effective medium formulism. We see that the extended Helmholtz stress tensor produces accurate optical force density. Note that in this case the Maxwell stress tensor within effective medium formulism produces almost the same result. This is because the effective permittivity and permeability

$|\varepsilon_t|, |\mu_t|$ are very close to 1 so that the extended Helmholtz and Maxwell stress tensors produce are almost identical results. When $|\varepsilon_t|, |\mu_t|$ deviate from 1, for example, in the case that the helices have a high dielectric cylinder core with relative permittivity $\varepsilon_c = 12.5$ as shown in the inset of Fig. 12(c), the Maxwell stress tensor will no longer give the correct description of optical force density. The comparison of the optical force densities calculated using different approaches is shown in Fig. 12(d). The Maxwell stress tensor gives the correct trend but not the magnitude of the optical force density while the results of the extended Helmholtz stress tensor are in accordance with that of the microscopic lattice.

Calculating the optical force density inside a medium is a difficult task as different macroscopic stress tensors give different results. There are multiple formulations of stress tensor and different experiments tend to support different stress tensors, which make the issue even more confusing [57–70]. Metamaterials actually offer a good platform to resolve some of those issues. If we consider a particular class of metamaterials, comprising an array of resonators in air, the microscopic structure is clearly specified and the optical force acting on each microscopic element can be calculated rigorously using stress tensor approach as we can always choose a contour in air surrounding the element. We can use the force acting on the microscopic element to define a force density for the macroscopic effective medium system. Using this approach, it has been shown that the Helmholtz stress tensor is the appropriate tensor for calculating the optical body/boundary forces of achiral metamaterials [44,52,53], other stress tensors cannot predict the force densities well because of the lack the electrostrictive and magnetostrictive terms and missing the information of microscopic lattice structure. We note that our method provides the electrostrictive and magnetostrictive tensor for bianisotropic metamaterials needed in the extended Helmholtz stress tensor and showed that this stress tensor can produce the most accurate optical force density. Therefore, our work not only provides a powerful tool to study the light-matter interaction for the bianisotropic metamaterial system, but also deepens our understanding of the light-induced force inside a complex medium.

VIII. SUMMARY

In summary, using multiple scattering theory, we derived closed-form expressions for the effective constitutive parameters and electro/magnetostrictive tensor components for 2D bianisotropic metamaterials. We also derived an expression for the extended electromagnetic stress tensor for these materials. The effective constitutive parameters can describe the optical scattering and absorption properties of bianisotropic metamaterials while the electro/magneto-strictive components, together with the extended electromagnetic stress tensor, provide sufficient information to determine the total optical force and the optical force density induced by external EM waves. We can use these macroscopic parameters to describe and predict the optical and optomechanical responses of complex man-made bianisotropic media, without the need to worry about the complex underlying structure. The results can also deepen our understanding of light-induced forces inside a complex medium and may find applications in optical manipulations, such as the optical stretching, compressing and sorting of materials.

ACKNOWLEDGMENTS

We thank Kun Ding, Ruo-Yang Zhang, and Xulin Zhang for valuable comments and suggestions. This work was supported by Hong Kong Research Grants Council through Grant No. AoE/P-02/12. S.W. was also supported by a grant from City University of Hong Kong (Project No. 9610388).

APPENDIX A: NUMERICAL CALCULATION OF THE EFFECTIVE CONSTITUTIVE PARAMETERS AND THEIR ELECTRO/MAGNETOSTRICTIVE TENSORS

The effective constitutive parameters of a photonic crystal can be obtained numerically by analyzing the eigenfields and the band dispersions in the long wavelength limit. For photonic crystals with chiral inclusions, there are two kinds of eigenfields corresponding to the lowest two bands. For each kind of eigenfields, its spatial average $\bar{\mathbf{E}}_j = 1/\Omega \int_\Omega \mathbf{E}_j dxdy$, $\bar{\mathbf{H}}_j = 1/\Omega \int_\Omega \mathbf{H}_j dxdy$ should fulfill the Maxwell equations [54]

$$\begin{aligned}\nabla \times (\bar{\mathbf{E}}_j e^{ik_j x}) &= i\omega \bar{\mathbf{B}}_j e^{ik_j x} = i\omega(\overleftrightarrow{\mu}\bar{\mathbf{H}}_j - i\overleftrightarrow{\kappa}\bar{\mathbf{E}}_j)e^{ik_j x},\\ \nabla \times (\bar{\mathbf{H}}_j e^{ik_j x}) &= -i\omega \bar{\mathbf{D}}_j e^{ik_j x} = -i\omega(\overleftrightarrow{\varepsilon}\bar{\mathbf{E}}_j + i\overleftrightarrow{\kappa}\bar{\mathbf{H}}_j)e^{ik_j x},\end{aligned} \tag{A1}$$

where k_j, $j = 1, 2$ is the magnitude of Bloch vector for each corresponding eigenfield, which can be complex numbers, $\hat{x}$ denotes the direction of the Bloch vector, $\overleftrightarrow{\varepsilon}$, $\overleftrightarrow{\mu}$ and $\overleftrightarrow{\kappa}$ are the effective constitutive parameters defined in Eq. (1) in main text. Then Eq. (A1) is reduced to

$$\begin{aligned} ik_j \begin{pmatrix} 0 \\ -E_{zj} \\ E_{yj} \end{pmatrix} &= i\omega \left[\begin{pmatrix} 0 \\ \mu_t H_{yj} \\ \mu_z H_{zj} \end{pmatrix} - i \begin{pmatrix} 0 \\ \kappa_t E_{yj} \\ \kappa_z E_{zj} \end{pmatrix} \right],\\ ik_j \begin{pmatrix} 0 \\ -H_{zj} \\ H_{yj} \end{pmatrix} &= -i\omega \left[\begin{pmatrix} 0 \\ \varepsilon_t E_{yj} \\ \varepsilon_z E_{zj} \end{pmatrix} + i \begin{pmatrix} 0 \\ \kappa_t H_{yj} \\ \kappa_z H_{zj} \end{pmatrix} \right], \end{aligned} \tag{A2}$$

where

$$\begin{aligned} \bar{\mathbf{E}}_j &= \frac{1}{\Omega}\int_\Omega \mathbf{E}_j dxdy = \begin{pmatrix} 0 \\ E_{yj} \\ E_{zj} \end{pmatrix},\\ \bar{\mathbf{H}}_j &= \frac{1}{\Omega}\int_\Omega \mathbf{H}_j dxdy = \begin{pmatrix} 0 \\ H_{yj} \\ H_{zj} \end{pmatrix}. \end{aligned} \tag{A3}$$

Solving Eq. (A2), the constitutive parameters can be obtained as

$$\begin{aligned} \varepsilon_z &= \frac{n_1 H_{y1} H_{z2} - n_2 H_{y2} H_{z1}}{E_{z2} H_{z1} - E_{z1} H_{z2}},\\ \varepsilon_t &= -\frac{n_1 H_{y2} H_{z1} - n_2 H_{y1} H_{z2}}{E_{y2} H_{y1} - E_{y1} H_{y2}}, \end{aligned} \tag{A4a}$$

$$\begin{aligned} \kappa_z &= i\frac{n_1 H_{y1} E_{z2} - n_2 H_{y2} E_{z1}}{E_{z2} H_{z1} - E_{z1} H_{z2}},\\ \kappa_t &= -i\frac{n_1 E_{y2} H_{z1} - n_2 E_{y1} H_{z2}}{E_{y2} H_{y1} - E_{y1} H_{y2}}, \end{aligned} \tag{A4b}$$

$$\mu_z = \frac{n_1 E_{y1} E_{z2} - n_2 E_{y2} E_{z1}}{E_{z2} H_{z1} - E_{z1} H_{z2}},$$
$$\mu_t = -\frac{n_1 E_{y2} E_{z1} - n_2 E_{y1} E_{z2}}{E_{y2} H_{y1} - E_{y1} H_{y2}}, \tag{A4c}$$
$$\kappa_z = -i\frac{n_1 E_{y1} H_{z2} - n_2 E_{y2} H_{z1}}{E_{z2} H_{z1} - E_{z1} H_{z2}},$$
$$\kappa_t = i\frac{n_1 H_{y2} E_{z1} - n_2 H_{y1} E_{z2}}{E_{y2} H_{y1} - E_{y1} H_{y2}}, \tag{A4d}$$

where $n_1 = k_1/\omega$ and $n_2 = k_2/\omega$ in the limit $k_{1,2} \to 0$ and $\omega \to 0$ are the effective refractive indices of the metamaterial. The two equations (A4b) and (A4d) about the chirality tensors always give the same result due to the relation between the two eigenfields.

We can repeat the calculation after deforming the unit cell, and the electrostrictive and magnetostrictive tensors can be obtained using the finite differences. For example, for the square lattice, we obtain the effective permittivity of the out-plane component before and after the unit cell being stretched using the Eq. (A4) as ε_z and $\varepsilon_z{}'$, then the electrostrictive term is given by

$$\frac{\partial \varepsilon_z}{\partial u_{xx}} = \frac{\varepsilon_z{}' - \varepsilon_z}{(2\Delta a/a)},$$

where a is the lattice constant, and Δa is an infinitesimal stretching displacement along the x direction, see Fig. 2.

APPENDIX B: CALCULATING COMPLEX K BLOCH BANDS FOR BIANISOTROPIC PHOTONIC CRYSTAL

When there is loss, to obtain the eigenfields and the corresponding Bloch K vectors, we need to calculate the complex K Bloch bands, which can be calculated using the Weak-Form-PDE module in COMSOL [71–73].

For bianisotropic medium possesses the following constitutive relations:

$$\mathbf{D} = \overleftrightarrow{\varepsilon}\varepsilon_0 \mathbf{E} + i\overleftrightarrow{\kappa}/c\mathbf{H}, \mathbf{B} = \overleftrightarrow{\mu}\mu_0 \mathbf{H} - i\overleftrightarrow{\kappa}/c\mathbf{E}, \tag{B1}$$

and if the constitutive parameters have diagonal matrix forms, the wave equations inside the medium are

$$\nabla \times [(\overleftrightarrow{\mu}^{-1}\overleftrightarrow{\kappa} - \overleftrightarrow{\kappa}^{-1}\overleftrightarrow{\varepsilon})^{-1}(i\overleftrightarrow{\mu}^{-1}\nabla \times \mathbf{E} + c\overleftrightarrow{\kappa}^{-1}\nabla \times \mathbf{H})]$$
$$= -\frac{\omega^2}{c^2}(\overleftrightarrow{\mu}\mathbf{H} - i\overleftrightarrow{\kappa}\mathbf{E}),$$
$$\nabla \times [(\overleftrightarrow{\kappa}^{-1}\overleftrightarrow{\mu} - \overleftrightarrow{\varepsilon}^{-1}\kappa)^{-1}(\overleftrightarrow{\kappa}^{-1}\nabla \times \mathbf{E} - i\overleftrightarrow{\varepsilon}^{-1}\nabla \times \mathbf{H})]$$
$$= \frac{\omega^2}{c^2}(\overleftrightarrow{\varepsilon}\mathbf{E} + i\overleftrightarrow{\kappa}\mathbf{H}). \tag{B2}$$

For the 2D system, because the transverse fields can be obtained from the z component fields according to the Maxwell equations, we only consider the z component fields. And using the Bloch theorem

$$E_z = u(\mathbf{r})\exp[-i(\omega t - \mathbf{k}\cdot\mathbf{r})],$$
$$H_z = v(\mathbf{r})\exp[-i(\omega t - \mathbf{k}\cdot\mathbf{r})], \tag{B3}$$

then the wave equations for z component fields are

$$(ik_x, ik_y) \times [f_1(u_y + ik_y u, -u_x - ik_x u) - i f_2(v_y + ik_y v, -v_x - ik_x v)]$$
$$+\nabla \times [f_1(u_y + ik_y u, -u_x - ik_x u) - i f_2(v_y + ik_y v, -v_x - ik_x v)] - i\frac{\omega^2}{c^2}(\mu_z v - i\kappa_z u) = 0, \tag{B4a}$$
$$(ik_x, ik_y) \times [i f_3(u_y + ik_y u, -u_x - ik_x u) + f_1(v_y + ik_y v, -v_x - ik_x v)]$$
$$+\nabla \times [i f_3(u_y + ik_y u, -u_x - ik_x u) + f_1(v_y + ik_y v, -v_x - ik_x v)] + i\frac{\omega^2}{c^2}(\varepsilon_z u + i\kappa_z v) = 0, \tag{B4b}$$

where

$$f_1 = \frac{\kappa_t}{\kappa_t^2 - \varepsilon_t\mu_t}, \quad f_2 = \frac{\mu_t}{\kappa_t^2 - \varepsilon_t\mu_t}, \quad f_3 = \frac{\varepsilon_t}{\kappa_t^2 - \varepsilon_t\mu_t},$$

and $u_x = \partial_x u$, $u_y = \partial_y u$, $v_x = \partial_x v$, $v_y = \partial_y v$. Multiplying the test functions $\tilde{u}$, $\tilde{v}$, respectively, and integrating within a unit cell, we then obtain the weak forms as

$$Wk(u) = (f_1 k^2 u + i f_1 k_x u_x + i f_1 k_y u_y - i f_2 k^2 v + f_2 k_x v_x + f_2 k_y v_y)\tilde{u} - (i f_1 k_x \tilde{u}_x u + i f_1 k_y \tilde{u}_y u - f_1 \tilde{u}_x u_x - f_1 \tilde{u}_y u_y$$
$$+ f_2 k_x \tilde{u}_x v + f_2 k_y \tilde{u}_y v + i f_2 \tilde{u}_x v_x + i f_2 \tilde{u}_y v_y) - i\frac{\omega^2}{c^2}(\mu v - i\kappa u)\tilde{u} = 0, \tag{B5a}$$
$$Wk(v) = (i f_3 k^2 u - f_3 k_x u_x - f_3 k_y u_y + f_1 k^2 v + i f_1 k_x v_x + i f_1 k_y v_y)\tilde{v} - (-f_3 k_x \tilde{v}_x u - f_3 k_y \tilde{v}_y u - i f_3 \tilde{v}_x u_x - i f_3 \tilde{v}_y u_y$$
$$+ i f_1 k_x \tilde{v}_x v + i f_1 k_y \tilde{v}_y v - f_1 \tilde{v}_x v_x - f_1 \tilde{v}_y v_y) + i\frac{\omega^2}{c^2}(\varepsilon u + i\kappa v)\tilde{v} = 0. \tag{B5b}$$

In the simulations, the fields should be approximated with Lagrange interpolation elements. The transverse component fields can be obtained according to the Maxwell equations, namely,

$$\begin{aligned} E_x &= i[-if_1(ik_y u + u_y) + f_2(ik_y v + v_y)]\exp[ik_x x + ik_y y], \\ E_y &= i[-if_1(-ik_x u - u_x) + f_2(-ik_x v - v_x)]\exp[ik_x x + ik_y y], \\ H_x &= i[-f_3(ik_y u + u_y) - if_1(ik_y v + v_y)]\exp[ik_x x + ik_y y], \\ H_y &= i[-f_3(-ik_x u - u_x) - if_1(-ik_x v - v_x)]\exp[ik_x x + ik_y y]. \end{aligned} \tag{B6}$$

Then knowing the complex Bloch K bands and the EM fields, we can numerically calculate the effective constitutive parameters and the electro/magnetostrictive tensors following the method proposed in Appendix A.

APPENDIX C: THE EQUALITY RELATIONSHIP BETWEEN THE MICROSCOPIC AND MACROSCOPIC ENERGY DENSITIES

In this part, we will show that from the spatial average relation between the microscopic and macroscopic fields, the equality relationship between the microscopic and macroscopic energy densities can be obtained. In the long wavelength limit, the effective fields (macroscopic fields) inside the effective medium are defined as the spatial average of the fields (microscopic fields) inside the metamaterial [54], namely,

$$\mathbf{E}_e = \frac{1}{\Omega}\int_\Omega \mathbf{E}d\Omega, \quad \mathbf{D}_e = \frac{1}{\Omega}\int_\Omega \mathbf{D}d\Omega, \tag{C1}$$

where Ω is the volume of the unit cell, $\mathbf{E}, \mathbf{D}$ and $\mathbf{E}_e, \mathbf{D}_e$ are the fields inside the metamaterial and effective medium, respectively. Starting from these relations, we will show that the energy density in the effective medium is also equal to the spatial average of the energy density inside the metamaterial, namely,

$$-\frac{1}{4}\mathbf{E}_e \cdot \mathbf{D}_e^* = -\frac{1}{4\Omega}\int_\Omega \mathbf{E}\cdot\mathbf{D}^* d\Omega. \tag{C2}$$

For the field in the metamaterial, according to the Maxwell equations and the long-wavelength limit where $\omega \to 0$ and $k \to 0$, we have

$$\nabla \times \mathbf{E} = i\omega\mathbf{B} \approx 0. \tag{C3}$$

That is, the electric field is a curl-free vector, therefore it can be written as gradient of a scalar,

$$\mathbf{E} = \nabla\phi. \tag{C4}$$

Substituting the relations into Eq. (C2), we have

$$\mathbf{E}_e = \frac{1}{\Omega}\int_\Omega \nabla\phi = \frac{1}{\Omega}\oint_\Gamma \phi\hat{n}d\Gamma, \tag{C5}$$

where $\mathbf{\Gamma}$ is the boundary of the unit cell and $\hat{n}$ is the unit normal vector of the boundary, and for the spatial average of electric energy in a unit cell, we have

$$\begin{aligned} -\frac{1}{4\Omega}\int_\Omega \mathbf{E}\cdot\mathbf{D}^* d\Omega &= -\frac{1}{4\Omega}\int_\Omega \nabla\phi\cdot\mathbf{D}^* d\Omega = -\frac{1}{4\Omega}\int_\Omega [\nabla\cdot(\phi\mathbf{D}^*) - \phi\nabla\cdot\mathbf{D}^*]d\Omega \\ &= -\frac{1}{4\Omega}\int_\Omega [\nabla\cdot(\phi\mathbf{D}^*)]d\Omega = -\frac{1}{4\Omega}\int_\Omega \phi\mathbf{D}^*\cdot\hat{n}d\Gamma, \end{aligned} \tag{C6}$$

where the Maxwell equation $\nabla\cdot\mathbf{D} = 0$ is used in the derivation.

In the following, we will take the cubic lattice as an example, other lattices can be followed in the same way. For the cubic lattice with lattice constant a, according to Eq. (C5), the electric field of each direction is given by

$$\begin{aligned} E_{ex} &= \frac{1}{\Omega}\oint_\Gamma \phi\hat{e}_x\cdot\hat{n}d\Gamma = \frac{1}{a^3}\int_0^a\int_0^a [\phi(a,y,z) - \phi(0,y,z)]dydz, \\ E_{ey} &= \frac{1}{\Omega}\oint_\Gamma \phi\hat{e}_y\cdot\hat{n}d\Gamma = \frac{1}{a^3}\int_0^a\int_0^a [\phi(x,a,z) - \phi(x,0,z)]dxdz, \\ E_{ez} &= \frac{1}{\Omega}\oint_\Gamma \phi\hat{e}_z\cdot\hat{n}d\Gamma = \frac{1}{a^3}\int_0^a\int_0^a [\phi(x,y,a) - \phi(x,y,0)]dxdz. \end{aligned} \tag{C7}$$

And note that

$$\begin{aligned} \frac{\partial}{\partial y}[\phi(a,y,z) - \phi(0,y,z)] &= E_y(a,y,z) - E_y(0,y,z) = E_y(0,y,z)(e^{ik_x a} - 1) = 0, \\ \frac{\partial}{\partial z}[\phi(a,y,z) - \phi(0,y,z)] &= E_z(a,y,z) - E_z(0,y,z) = E_z(0,y,z)(e^{ik_x a} - 1) = 0, \end{aligned}$$

where the long-wavelength limit that $k_x \to 0$, $k_y \to 0$, and $k_z \to 0$ are used in the derivations. It means that the functions in the brackets of Eq. (C7) are independent with the coordinates and can be picked out. Thus the effective electric field can be

rewritten as

$$\begin{aligned} E_{ex} &= \frac{1}{a^3}\int_0^a\int_0^a [\phi(a,y,z)-\phi(0,y,z)]dydz = \frac{1}{a}[\phi(a,y,z)-\phi(0,y,z)] = \frac{1}{a}\int_0^a E_x dx, \\ E_{ey} &= \frac{1}{a^3}\int_0^a\int_0^a [\phi(x,a,z)-\phi(x,0,z)]dxdz = \frac{1}{a}[\phi(x,a,z)-\phi(x,0,z)] = \frac{1}{a}\int_0^a E_y dy, \\ E_{ez} &= \frac{1}{a^3}\int_0^a\int_0^a [\phi(x,y,a)-\phi(x,y,0)]dxdz = \frac{1}{a}[\phi(x,y,a)-\phi(x,y,0)] = \frac{1}{a}\int_0^a E_z dz. \end{aligned} \tag{C8}$$

And for the electric displacement, take the D_{ex} as an example, we use the integration by part that

$$\begin{aligned} D_{ex} &= \frac{1}{a^3}\iiint_\Omega D_x(x,y,z)dxdydz = \frac{1}{a^3}x\iint D_x(x,y,z)dydz\Big|_0^a - \frac{1}{a^3}\int_0^a\left[x\frac{\partial}{\partial x}\iint D_x(x,y,z)dydz\right]dx \\ &= \frac{1}{a^2}\iint D_x(a,y,z)dydz - \frac{1}{a^3}\int_0^a\left[x\iint\frac{\partial}{\partial x}D_x(x,y,z)dydz\right]dx \\ &= \frac{1}{a^2}\iint D_x(a,y,z)dydz + \frac{1}{a^3}\int_0^a\left\{x\iint\left[\frac{\partial}{\partial y}D_y(x,y,z)+\frac{\partial}{\partial z}D_z(x,y,z)\right]dydz\right\}dx \\ &= \frac{1}{a^2}\iint D_x(a,y,z)dydz + \frac{1}{a^3}\int_0^a\left\{x\int_0^a[D_y(x,a,z)-D_y(x,0,z)]dz\right\}dx \\ &\quad + \frac{1}{a^3}\int_0^a\left\{x\int_0^a[D_z(x,y,a)-D_z(x,y,0)]dy\right\}dx = \frac{1}{a^2}\iint D_x(a,y,z)dydz. \end{aligned} \tag{C9}$$

Here we used that $\nabla\cdot\mathbf{D} = \partial D_x/\partial x + \partial D_y/\partial y + \partial D_z/\partial z = 0$ and $\mathbf{D}(x,y,a) = \mathbf{D}(x,y,0)e^{ik_z a} = \mathbf{D}(x,y,0)$ in the derivations. The same procedure can be done for other components. Then according to Eqs. (C8) and (C9), we can summarize that

$$E_{ei} = \frac{1}{a}\int_0^a \mathbf{E}\cdot d\mathbf{x}_i, \qquad D_{ei} = \frac{1}{a^2}\iint \mathbf{D}\cdot d\mathbf{S}_i, \tag{C10}$$

which is just the homogenization theory proposed by J. B. Pendry [74].

Substituting the relations (C10) into Eq. (C6), we can further obtain the relation between the electric energy densities,

$$\begin{aligned} -\frac{1}{4\Omega}\int_\Omega \mathbf{E}\cdot\mathbf{D}^* d\Omega &= -\frac{1}{4\Omega}\int_\Omega \phi\mathbf{D}^*\cdot\hat{n}d\Gamma \\ &= -\frac{1}{4a^3}\left\{\int_0^a\int_0^a[\phi(a,y,z)D_x^*(a,y,z)-\phi(0,y,z)D_x^*(0,y,z)]dydz\right. \\ &\quad + \int_0^a\int_0^a[\phi(x,a,z)D_y^*(x,a,z)-\phi(x,0,z)D_y^*(x,0,z)]dxdz \\ &\quad \left.+ \int_0^a\int_0^a[\phi(x,y,a)D_z^*(x,y,a)-\phi(x,y,0)D_z^*(x,y,0)]dxdy\right\} \\ &= -\frac{1}{4a^3}\left\{[\phi(a,y,z)-\phi(0,y,z)]\int_0^a\int_0^a D_x^*(a,y,z)dydz\right. \\ &\quad + [\phi(x,a,z)-\phi(x,0,z)]\int_0^a\int_0^a D_y^*(x,a,z)dxdz \\ &\quad \left.+ [\phi(x,y,a)-\phi(x,y,0)]\int_0^a\int_0^a D_z^*(x,y,a)]dxdy\right\} \\ &= -\frac{1}{4}(E_{ex}D_{ex}^* + E_{ey}D_{ey}^* + E_{ez}D_{ez}^*) = -\frac{1}{4}\mathbf{E}_e\cdot\mathbf{D}_e^*, \end{aligned} \tag{C11}$$

which is just what we desired. Similarly, we can also obtain

$$-\frac{1}{4\Omega}\int_\Omega \mathbf{H}\cdot\mathbf{B}^* d\Omega = -\frac{1}{4}\mathbf{H}_e\cdot\mathbf{B}_e^*$$

for the magnetic component.

[1] R. A. Shelby, D. R. smith, and S. Schultz, Science **292**, 77 (2001).
[2] J. B. Pendry, Phys. Rev. Lett. **85**, 3966 (2000).
[3] J. B. Pendry, D. Schurig, and D. R. Smith, Science **312**, 1780 (2006).
[4] D. Schurig, J. J. Mock, B. J. Justice, S. A. Cummer, J. B. Pendry, A. F. Starr, and D. R. Smith, Science **314**, 977 (2006).
[5] W. Cai, U. K. Chettiar, A. V. Kildishev, and V. M. Shalaev, Nat. Photon. **1**, 224 (2007).
[6] H. Chen and C. T. Chan, Appl. Phys. Lett. **91**, 183518 (2007).
[7] M. Silveirinha and N. Engheta, Phys. Rev. Lett. **97**, 157403 (2006).
[8] X. Huang, Y. Lai, Z. H. Hang, H. Zheng, and C. T. Chan, Nat. Mater. **10**, 582 (2011).
[9] A. Priou, A. Sihvola, and S. Tretyakow, *Advances in Complex Electromagnetic Materials* (Springer Science & Business Media, 2012).
[10] A. H. Sihvola and Olli P. M. Pekonen, J. Phys. D: App. Phys. **29**, 514 (1996).
[11] G. W. Milton, *The Theory of Composites* (Cambridge University Press, Cambridge, 2002).
[12] J. Jin, S. Liu, Z. Lin, and S. T. Chui, Phys. Rev. B **80**, 115101 (2009).
[13] J. A. Reyes-Avendaño, U. Algredo-Badillo, P. Halevi, and F. Pérez-Rodríguez, New J. Phys. **13**, 073041 (2011).
[14] C. Fietz, J. Opt. Soc. Am. B **30**, 1937 (2013).
[15] X. Zhang and Y. Wu, Sci. Rep. **5**, 7892 (2015).
[16] J. B. Pendry, Science **306**, 1353 (2004).
[17] S. Zhang, Y. S. Park, J. Li, X. Lu, W. Zhang, and X. Zhang, Phys. Rev. Lett. **102**, 023901 (2009).
[18] C. Wu, H. Li, Z. Wei, X. Yu, and C. T. Chan, Phys. Rev. Lett. **105**, 247401 (2010).
[19] E. Plum, V. A. Fedotov, A. S. Schwanecke, and N. I. Zheludev, Appl. Phys. Let. **90**, 223113 (2007).
[20] H. Liu, D. A. Genov, D. M. Wu, Y. M. Liu, Z. W. Liu, C. Sun, S. N. Zhu, and X. Zhang, Phys. Rev. B **76**, 073101 (2007).
[21] T. Q. Li, H. Liu, T. Li, S. M. Wang, F. M. Wang, R. X. Wu, P. Chen, S. N. Zhu, and X. Zhang, Appl. Phys. Lett. **92**, 131111 (2008).
[22] S. L. Prosvirnin and N. I. Zheludev, Phys. Rev. E **71**, 037603 (2005).
[23] V. A. Fedotov, P. L. Mladyonov, S. L. Prosvirnin, A. V. Rogacheva, Y. Chen, and N. I. Zheludev, Phys. Rev. Lett. **97**, 167401 (2006).
[24] E. Plum, X.-X. Liu, V. A. Fedotov, Y. Chen, D. P. Tsai, and N. I. Zheludev, Phys. Rev. Lett. **102**, 113902 (2009).
[25] A. B. Khanikaev, S. H. Mousavi, W.-K. Tse, M. Kargarian, A. H. MacDonald, and G. Shevets, Nat. Mater. **12**, 233 (2013).
[26] W. Gao, M. Lawrence, B. Yang, F. Liu, F. Fang, B. Beri, J. Li and S. Zhang, Phys. Rev. Lett. **114**, 037402 (2015).
[27] X. Chen, B.-I. Wu, J. A. Kong, and T. M. Grzegorczyk, Phys. Rev. E **71**, 046610 (2005).
[28] Z. Li, K. Aydin, and E. Ozbay, Phys. Rev. E **79**, 026610 (2009).
[29] C. Menzel, C. Rockstuhl, T. Paul, and F. Lederer, Appl. Phys. Lett. **93**, 233106 (2008).
[30] B. Wang, J. Zhou, T. Koschny, M. Kafesaki, and C. M. Soukoulis, J. Opt. A: Pure Appl. Opt. **11**, 114003 (2009).
[31] R. Zhao, T. Koschny, and C. M. Soukoulis, Opt. Express **18**, 14553 (2010).
[32] J. Guck, R. Ananthakrishnan, T. J. Moon, C. C. Cunningham, and J. Kas, Phys. Rev. Lett. **84**, 5451 (2000).
[33] J. Guck, R. Ananthakrishnan, H. Mahmood, T. J. Moon, C. C. Cunningham, and J. Kas, Biophys. J. **81**, 767 (2001).
[34] B. F. Kennedy, P. Wijesinghe, and D. D. Sampson, Nat. Photon. **11**, 215 (2017).
[35] Y. Wu, J. Li, Z.-Q. Zhang, and C. T. Chan, Phys. Rev. B **74**, 085111 (2006).
[36] B. A. Slovick, Z. G. Yu, and S. Krishnamurthy, Phys. Rev. B **89**, 155118 (2014).
[37] J. M. MacLaren, S. Crampin, D. D. Vvedensky, and J. B. Pendry, Phys. Rev. B **40**, 12164 (1989).
[38] A. Modinos, N. Stefanou, and V. Yannopapas, Opt. Express **8**, 197 (2001).
[39] J. M. MacLaren, X. G. Zhang, W. H. Butler, and X. Wang, Phys. Rev. B **59**, 5470 (1999).
[40] C. F. Bohren and D. R. Huffman, *Absorption and Scattering of Light by Small Particles* (Wiley and Sons, New York, 1983).
[41] M. Abramowitz and I. A. Stegun, *Handbook of Mathematical Functions with Formulas, Graphs, and Mathematical Tables* (Wiley, New York, 1972).
[42] Y. Wu and Z. Q. Zhang, Phys. Rev. B **79**, 195111 (2009).
[43] S. K. Chin, N. A. Nicorovici, and R. C. McPhedran, Phys. Rev. E **49**, 4590 (1994).
[44] W. Sun, S. B. Wang, J. Ng, L. Zhou, and C. T. Chan, Phys. Rev. B **91**, 235439 (2015).
[45] A. H. Sihvola and I. V. Lindell, Electron. Lett. **26**, 118 (1990).
[46] A. Lakhtakia, V. K. Varadan, and V. V. Varadan, J. Mater. Res. **8**, 917 (1993).
[47] P. Penfield, and H. A. Haus, *Electrodynamics of Moving Media* (MIT Press, Cambridge, 1967).
[48] L. D. Landau and E. M. Lifshitz, *Theory of Elasticity*, 3rd ed. (Butterworth-Heinemann, New York, 1986).
[49] R. A. Anderson, Phys. Rev. B **33**, 1302 (1986).
[50] Y. M. Shkel and D. J. Klingenberg, J. Appl. Phys. **80**, 4566 (1996).
[51] L. D. Landau, E. M. Lifshitz, and L. P. Pitaevskii, *Electrodynamics of Continuous Media*, 2nd ed. (Butterworth-Heinemann, New York, 1984).
[52] S. Wang, J. Ng, M. Xiao, and C. T. Chan, Sci. Adv. **2**, e1501485 (2016).
[53] N. Wang, S. Wang, and J. Ng, Phys. Rev. A **97**, 033839 (2018).
[54] M. G. Silveirinha, Phys. Rev. B **75**, 115104 (2007).
[55] www.comsol.com.
[56] H. Helmholtz, Ann. Phys. **249**, 385 (1881).
[57] H. Minkowski, Nachr. Ges. Wiss. Goettingen, Math.-Phys. Kl. **1**, 53 (1908).
[58] M. Abraham, Rend. Circ. Mat. Palermo **28**, 1 (1909).
[59] A. Einstein and J. Laub, Ann. Phys. **331**, 541 (1908).
[60] M. Mansuripur, A. R. Zakharian, and E. M. Wright, Phys. Rev. A **88**, 023826 (2013).
[61] I. Liberal, I. Ederra, R. Gonzalo, and R. W. Ziolkowski, Phys. Rev. A **88**, 053808 (2013).
[62] A. M. Jazayeri and K. Mehrany, Phys. Rev. A **89**, 043845 (2014).
[63] M. Bethune-Waddell and K. J. Chau, Rep. Pro. Phys. **78**, 122401 (2015).
[64] K. J. Webb, Phys. Rev. B **94**, 064203 (2016).
[65] C. J. Sheppard and B. A. Kemp, Phys. Rev. A **93**, 013855 (2016).
[66] I. Brevik, Phys. Rep. **52**, 133 (1979).

[67] G. L. J. A. Rikken and B. A. van Tiggelen, Phys. Rev. Lett. **108**, 230402 (2012).
[68] N. G. C. Astrath, L. C. Malacarne, M. L. Baesso, G. V.B. Lukasievicz, and S. E. Bialkowski, Nat. Commun. **5**, 4363 (2014).
[69] C. W. Qiu, W. Ding, M. R. C. Mahdy, D. Gao, T. Zhang, F. C. Cheong, A. Dogariu, Z. Wang, and C. T. Lim, Light Sci. Appl. **4**, e278 (2015).
[70] B. A. Kemp, Nat. Photon. **10**, 291 (2016).
[71] M. Davanc, Y. Urzhumov, and G. Shvets, Opt. Express **15**, 9681 (2007).
[72] M. Davanc, Y. Urzhumov, and G. Shvets, Opt. Express **19**, 19027 (2011).
[73] J.-M. Jin, *The Finite Element Method in Electromagnetics* (Wiley, Hoboken, 2014).
[74] D. R. Smith and J. B. Pendry, J. Opt. Soc. Am. B. **23**, 391 (2006).